RSC Advances

This is an *Accepted Manuscript*, which has been through the Royal Society of Chemistry peer review process and has been accepted for publication.

Accepted Manuscripts are published online shortly after acceptance, before technical editing, formatting and proof reading. Using this free service, authors can make their results available to the community, in citable form, before we publish the edited article. This *Accepted Manuscript* will be replaced by the edited, formatted and paginated article as soon as this is available.

You can find more information about *Accepted Manuscripts* in the Information for Authors.

Please note that technical editing may introduce minor changes to the text and/or graphics, which may alter content. The journal's standard Terms & Conditions and the Ethical guidelines still apply. In no event shall the Royal Society of Chemistry be held responsible for any errors or omissions in this *Accepted Manuscript* or any consequences arising from the use of any information it contains.

ROYAL SOCIETY OF CHEMISTRY

www.rsc.org/advances

Cite this: DOI: 10.1039/c0xx00000x

www.rsc.org/xxxxxx

ARTICLE TYPE

Supramolecular Analyte Recognition: Experiment Theory Interplay

Paramjit Kaur* and Kamaljit Singh*

Received (in XXX, XXX) Xth XXXXXXXXX 20XX, Accepted Xth XXXXXXXXX 20XX
DOI: 10.1039/b000000x

Due to a large impact of analyte recognition in biology and environment, the development of supramolecular recognition and sensing strategies has attracted a considerable interest in the recent years. Although researchers employ a variety of spectroscopic (optical and or fluorescence) and/or the analytical techniques based on changes in mass, electrochemical behaviour and other changes to assess the perturbation of physico-chemical changes associated with a supramolecular sensing event, theoretical calculations have proven to be a pivotal tool to substantiate the experimental results. Such calculations assume additional significance as the information gained in such calculations can help designing new, even more efficient chemosensors and the time and resources consumed in the synthesis of sensors and associated trials, errors and operational difficulties are considerably reduced. This review presents some supramolecular sensing events wherein the sensing mechanism is supported by theoretical predictions of the binding modes based on the perturbations in the energies of the frontier molecular orbitals upon recognition of the guest species.

1. Introduction

Owing to the influence of various anions and cations in our daily life, the design and development of the molecular receptors possessing the ability to selectively recognize analytes and signal a quantifiable response, has emerged as an active area of research. The molecular sensors are generally composed of a selective receptor and a signaling subunit. The function of the receptor is to recognize an analyte mainly through supramolecular interactions; the signalling sub unit transduces the response by a signal output in terms of color change, emission change (enhancement or quenching of emission intensity) and the redox shifts etc.[1] Consequent to this, the supramolecular molecular sensors have attained a special status owing to their implication in the fabrication of the sensing devices. For instance, the receptors which exhibit color and the emission changes in the presence of a guest species, have emerged as ideal candidates for use in the optical fibre devices, whereas the redox active molecular sensors signaling redox changes upon addition of analytes, can find applications in the development of amperometric sensing devices etc. In general, the binding/interaction of the receptor with the analyte can modulate (i) UV-visible absorption properties of the former which is manifested in terms of bathochromic or hypsochromic shifts in the absorption bands responsible for "naked-eye" color changes during a sensing event, (ii) fluorescence properties of the receptor manifested as enhanced/quenched/shifted or appearance of new emission band(s), and (iii) redox properties of the receptor in terms of shifts (cathodic or anodic) in the redox potentials of the receptor and/or appearance of new peaks. Such changes are measurable and quantifiable leading to wealth of information regarding binding constants, stoichiometry and formation receptor-analyte species, limit of detection, sensitivity as well as selectivity of the sensing process. Theoretical calculations have been frequently used as a robust tool to substantiate the proposed binding hypothesis and have thus gained significance. Optimization of molecular structure and geometry, evaluation of the energies of the participating frontier molecular orbitals (FMOs), highest occupied and lowest unoccupied molecular orbitals (HOMO and LUMO, respectively) of the receptor, assignment and correlation of the molecular electronic transitions, atomic charges etc. provide an in-depth insight into the understanding of the sensing mechanism and these studies can also help to design more efficient sensors. The current review provides an overview of the representative work during the recent past mainly 2009 to 2012, wherein the experimental results of the supramolecular sensing events have been supported by such calculations and the binding mechanisms have been unequivocally suggested.

2. Cation recognition

2.1 Charge transfer (CT) based systems

A coumarin-based fluorogenic probe bearing a 2-picolyl unit **1** was developed[2] as a chemosensor for Cu^{2+} (Fig. 1), wherein quenching of fluorescence of the coumarin moiety after complexation with Cu^{2+} via ligand to metal d-orbital and/or ligand to metal charge-transfer (LMCT) was proposed to be the operative mechanism. In order to gain deeper insight in understanding what type of energy changes the frontier orbitals of **1** undergo upon interaction with the guest, *ab initio* calculations suggested the mechanism wherein, LMCT having main contribution from HOMO→LUMO+4 (18%) and

RSC Advances Accepted Manuscript

HOMO→LUMO+6 (11%) excitations from the coumarin moiety to Cu^{2+} centre, provides a pathway for non-radiative deactivation of excited state which in fact, is one of the causes of the observed quenching of the fluorescence emission.

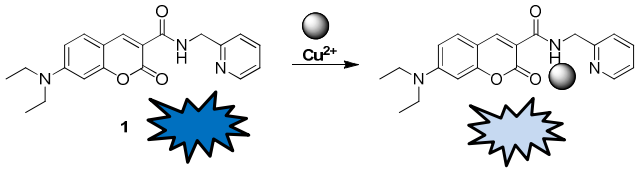

Fig. 1 Coumarin based fluorogenic probe for Cu^{2+} detection.

A semisquarylium dye **2** was found to be highly selective for Hg^{2+} ions.[3] The intensity of both the absorption and the emission bands of the dye decreased in the presence of Hg^{2+} ions, and was attributed to the formation of a 2:1 (**2**:Hg^{2+}) coordination complex during the sensing event (Fig. 2). The formation of the complex is supported by calculated geometry indicating bridging of the Hg^{2+} ion between the sulfur atom and the carbonyl oxygen atom. Calculation of electron distribution in the HOMO and LUMO orbitals of the dye revealed that HOMO-LUMO excitation displaced the electron density from the thiazole moiety to the cyclobutene moiety reflecting a strong intramolecular charge-transfer (ICT) character of the dye (Fig. 3).

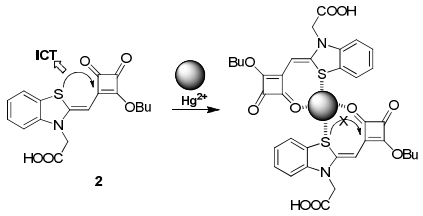

Fig. 2 Complexation of Hg^{2+} by semisquarylium dye.

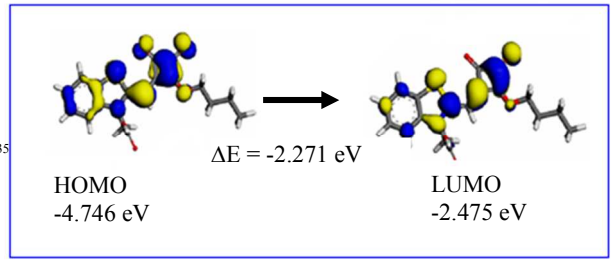

Fig. 3 Electron density distribution of HOMO and LUMO energy levels of the **2** [Reprinted with permission from ref. **3**. Copyright 2009 Elsevier].

Complexation with Hg^{2+} via sulfur atom of thiazole reduces the electron donating ability of thiazole moiety restricting the ICT, thus causing the observed spectral changes.

A donor (D)-π-acceptor (A) system **3** has been developed as a chemosensor for Ni^{2+}.[4] The D-A dyad **3** exhibits ICT, supported by DFT calculations. The comparison of the electron distribution in the FMOs revealed that the HOMO-LUMO excitation displaced the electron density from the donor unit 4-[bis(pyridin-2-ylmethyl)amino] to the isophrone moiety (Fig. 4a). The observed hypsochromic shift in the absorption band of **15** in the presence of Ni^{2+} has been attributed to the formation of a complex via N atoms of the donor unit and thereby restricting the ICT (Fig. 4b).

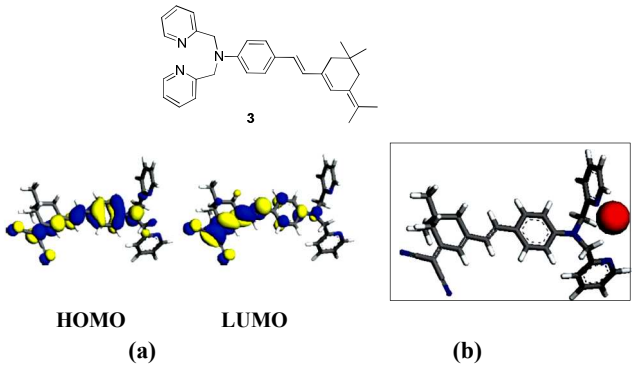

Fig. 4 (a) Electron density distribution of HOMO and LUMO energy levels of **3** and (b) the energy minimised structure of **3**:Ni^{2+} complex [Reproduced from ref. **4** by permission of the publisher (Taylor and Francis Ltd. http:/www.tandf.co.uk/journals].

The recognition of the guests by a D-A type dyads is generally manifested by either a hypochromic or bathochromic shift in the ICT band arising from an electronic transition between appropriate HOMO and LUMO, or observes no shift at all depending upon the participation of the coordination sites. If the guest coordinates to the donor site, it would lead to hypsochromic shift, whereas binding to the acceptor site facilitates a bathochromic shift. A weak interaction with either of these two may not shift the ICT band at all and show only hypochromic effect (reduction in the intensity). In line with this, very convincingly, Martinez-Manez et. al.[5] have evaluated the cation binding behaviour of **4-9** possessing the ICT. The DFT calculations performed on the model compound **4** predicted the main absorption band due to electron transfer from the HOMO orbitals of the N,N-dimethylaniline donor unit to the LUMO orbitals of the thiazole unit (Fig. 5). The hypsochromic, bathochromic and hypochromic effects exhibited by the derivatives in the presence of Hg^{2+}, Pb^{2+}, Fe^{3+} etc. has been attributed to the coordination site preference by the metal ions.

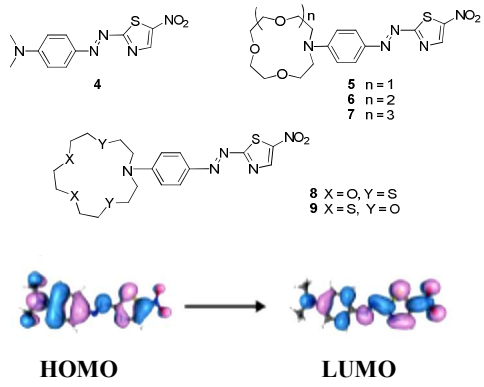

Fig. 5 The electron density distribution of HOMO and LUMO energy levels of **4** [Reproduced with permission from (ref. 5). Copyright (2011) Wiley-VCH].

The perturbation in the absorption spectral pattern upon complexation was well supported by the DFT calculations. Thus,

RSC Advances Accepted Manuscript

This journal is © The Royal Society of Chemistry [year]

the interaction of **4** with Hg^{2+} was proposed with the aniline and thiazole units. When Hg^{2+} was coordinated by the nitrogen atoms of azo-thiazole moiety, the TD-DFT calculations predicted the intense ICT (responsible for bathochromic shift), while, the coordination at the aniline centre predicted the hypsochromic shift giving band at lower wave length (Fig. 6).

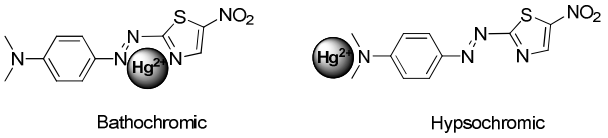

Fig. 6 Coordination modes and colorimetric behaviour of **4** with Hg^{2+} .

Taking advantage of coordinative perturbations in the ICT, our research group has developed a series of hetarylazo derivatives **10-13** as chemosensors for the detection of Zn^{2+}, Hg^{2+}, Fe^{3+}, Cu^{2+}, Pb^{2+} and Co^{2+} based upon the visual as well as absorption spectral changes.[6-9] The "*push-pull*" chromophore **10** possessing electron donating N,N-di(β-ethoxycarbonylethyl)aniline group and electron withdrawing thiadiazole moiety manifests its preference for Hg^{2+} and Fe^{3+} over other metal ions in the form of bathochromically shifted twin absorption band.[6] The bathochromic shift has been attributed to the facilitated ICT prevailing in **10**, suggested to be a result of interaction of metal ions with the sulfur atom of the thiadiazole and the nitrogen atom of the azo linkage. The proposed binding mode was well corroborated by DFT calculations. The energy minimized structure of **10** with Hg^{2+} depicted the interaction of Hg^{2+} with the sulfur atoms of the thiadiazole rings and the azo nitrogen atoms of two molecules of **10**, resulting in a 2:1 stoichiometry of the resulting complex, which was also supported by the predicted 2:1 stoichiometry from the Job's plot. However with Fe^{3+}, the best optimized structure predicted the same binding mode but with 1:1 stoichiometry as supported by the Job's plot (Fig. 7). TD-DFT calculations further established the HOMO-1→LUMO+1 as the main contributing transition to the bathochromically shifted band in case of recognition of Hg^{2+} and Fe^{3+} with a small contribution from the HOMO→LUMO transition (corresponding to one with longer wavelength in the twin band) in case of Hg^{2+}, and H-3→L (corresponding to the one with shorter wavelength in the twin band) in case of Fe^{3+} detection (Fig. 8).

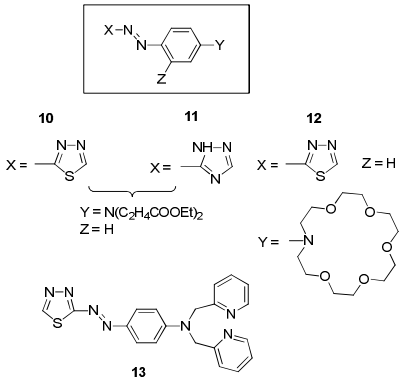

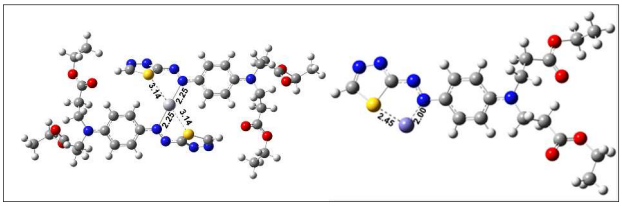

Fig. 7 The energy minimised structures of (a) $(\mathbf{10})_2$:Hg^{2+} and (b) **10**:Fe^{3+} complexes.

Structurally similar "*push-pull*" system **11**, with a triazole moiety as electron withdrawing group, also exhibited a bathochromically shifted absorption band in the presence of Cu^{2+}.[7] Like **10**, the bathochromically shifted low energy ICT band is suggestive of binding of Cu^{2+} with the triazole moiety getting support from the DFT calculations (Fig. 9).

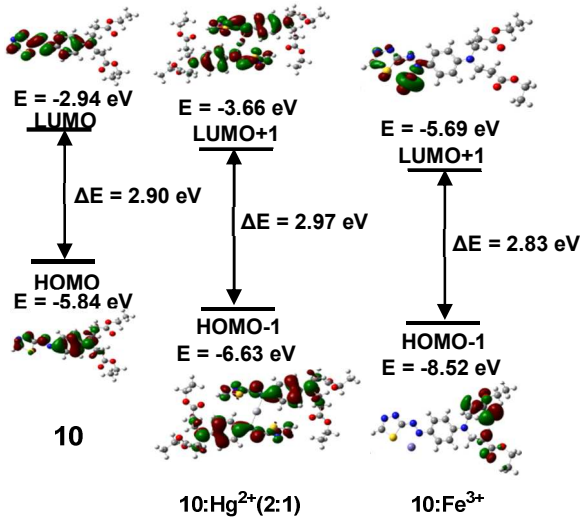

Fig.8 Comparative energy level diagram of the main transitions (absorption) alongwith the participating FMOs (isovalue = 0.03).

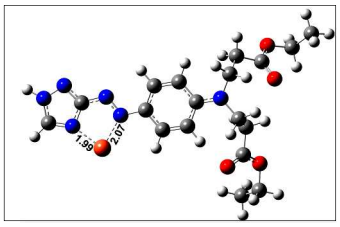

Fig. 9 Energy minimised structure of **11**:Cu^{2+} complex.

The energy minimized structure supports the 1:1 stoichiometry of the complex as established by the Job's plot. The TD-DFT calculations predict the H-3→L and H-1→L transitions as the main contributors to the bathochromically shifted low energy absorption band responsible for the color change in **11**:Cu^{2+} complex (Fig. 10). Further the receptor **12** behaved differently in the sense that the inclusion of aza crown moiety induced a change in selectivity when compared to receptor **10**.[8] The significant feature was that the low energy ICT band of **12** exhibited contrasting behaviour in the presence of Hg^{2+} and Pb^{2+}.

RSC Advances Accepted Manuscript

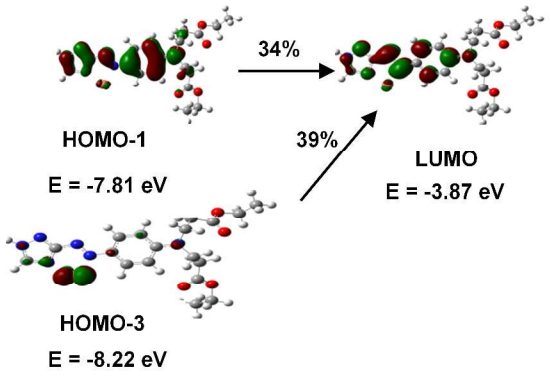

Fig. 10 The energy level diagram of the main transitions (absorption) observed in **11**:Cu^{2+} complex, along with the participating FMOS (isovalue 0.03).

In the presence of Hg^{2+}, a bathochromic shift in the ICT was noted, whereas in the presence of Pb^{2+}, a hypsochromic shift was observed. The shift in case of Hg^{2+} could be ascribed to the interaction of Hg^{2+} with the 1,3,4-thiadiazole ring and azo nitrogen atom similar to that found for the receptor **10**. On the other hand, the hypsochromic shift in case of Pb^{2+} suggested the interaction with the lone pair of the nitrogen and oxygen atoms of the aza crown group. The proposed binding modes and the resultant effects on the absorption spectrum were also confirmed by performing DFT calculations on the metal complexes (Fig. 11).

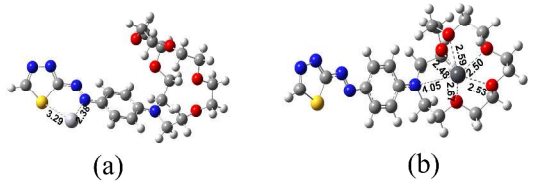

Fig.11 The energy minimised structures of (a) 12:Hg^{2+} and (b) 12:Pb^{2+} complexes.

The experimental results were in good agreement to the TD-DFT studies. While in **12**:Hg^{2+}, the twin absorption band is seen to be contributed largely by H→L transition (64%) and to a lesser extent by H→L+1 transition (36%), whereas in **12**:Pb^{2+}, H→L transition is the sole contributor to its main ICT band. On comparison to that with free **12**, it could be seen that the predominant characteristic band in all the three cases, i.e., **12**, **12**:Hg^{2+} and **12**:Pb^{2+}, originates from H→L transition, albeit having different energies (Fig. 12). The receptor **13** responded to Cu^{2+}, Co^{2+} and Hg^{2+} in terms of exhibiting hypsochromic shift in its low energy ICT band (Cu^{2+}>Co^{2+}>Hg^{2+}) hinting at the coordination of metal ions involving the two pyridine as well as aniline nitrogen atoms of the donor site.[9]The proposed binding mode as well as the order of hypsochromic shift, were well validated with the help of *ab initio* calculations. The predicted bond lengths indicate the weak interaction of Hg^{2+} with the ligating atoms in the binding pocket as compared to Cu^{2+} and Co^{2+}. The order of the binding constants determined experimentally was in good agreement with the calculated ΔG values (Fig. 13).

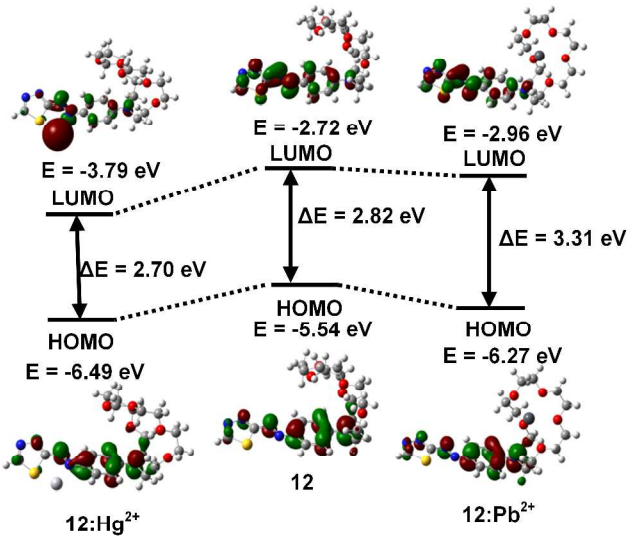

Fig. 12 Comparative energy level diagram of main transitions along with the participating FMOs (isovalue = 0.030).

Further, the TD-DFT calculations performed on **13**:M^{2+} complexes provided an insight into the nature of the transitions corresponding to the main ICT absorption bands obtained experimentally and the data is presented in Table 1. In case of **13**:Cu^{2+}, as evident from the FMOs (Fig. 14a), the electron density for HOMO, HOMO-3 and HOMO-7 was dispersed on to Cu^{2+} also. It was thus proposed that this dispersal could be a cause for observed hypsochromic shift in the low energy band, and also the band was regarded as a combination of ICT/MLCT (metal to ligand charge transfer). Since similar dispersal of one of the contributing orbitals, HOMO-1, was also observed in Co^{2+} (Fig. 14b), the hypsochromically shifted band was regarded as a combination of ICT/MLCT like in case of Cu^{2+} recognition. However, no such dispersal was predicted in case of **13**:Hg^{2+} (Fig. 14c), and the band was assigned to be of ICT nature only. This difference in the nature of the main absorption band was attributed to the open shell nature of Cu^{2+} and Co^{2+} in comparison to the close shell nature of Hg^{2+}.

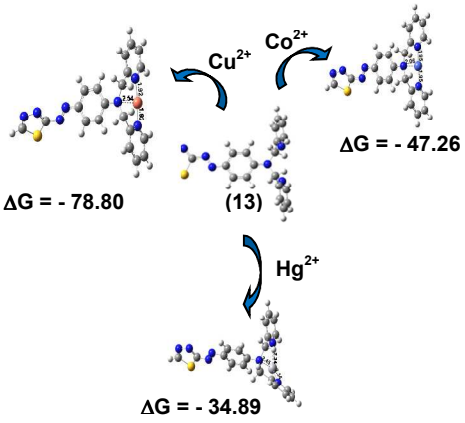

Fig. 13 The energy minimised structures of **13**, **13**:Cu^{2+}, **13**:Co^{2+}, and **13**:Hg^{2+} along with the respective ΔG (KJ/mol) values.

Further, the resulted hypsochromic shift due to dispersal of HOMOs electron density was further supported by the natural

RSC Advances Accepted Manuscript

This journal is © The Royal Society of Chemistry [year]

bond orbital (NBO) calculations, which indicated the decreased negative charge on the donor part on complexation with the metal ions, unequivocally suggesting the presence of M^{2+} ions in the binding pocket created by the pyridyl and the aniline nitrogens, hence preventing the ICT.

Table 1 Assignment of the main absorption transitions on the complexes on the basis of TD-DFT calculations.

S. No.	Complex	Hypsochromically shifted band at λ(nm)	Main contributory transitions
1.	**13**:Cu^{2+}	352	HOMO-3→LUMO(30%), HOMO-11→LUMO(10%), HOMO-7→LUMO(9%), HOMO→LUMO(5%)
2.	**13**:Co^{2+}	370	HOMO-3→LUMO(32%), HOMO-1→LUMO+1(24%), HOMO-5→LUMO(11%)
3.	**13**:Hg^{2+}	400	HOMO-1→LUMO(100%)

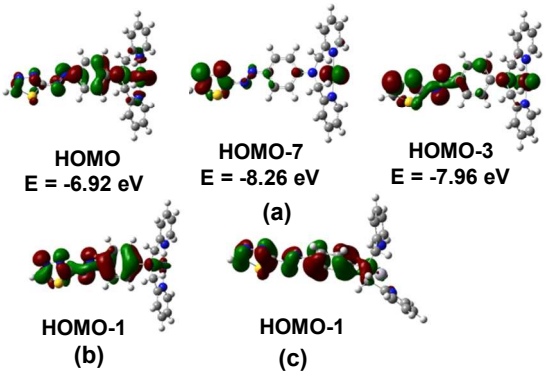

Fig. 14 The electron density distribution of various energy levels of (a) **13**:Cu^{2+}, (b) **13**:Co^{2+} and (c) **13**:Hg^{2+} complexes.

Similarly, in another investigation,[10] we have reported the perturbations in the strong ICT exhibited by **14** as a result of electrophilic substitution reaction of Hg^{2+} resulting in the formation of a covalently linked Hg^{2+} complex. The formation of the product was well corroborated by the DFT calculations predicting the changes in the respective C-C bond lengths expected to be affected by covalent bonding as shown in Fig. 15. The NBO calculations were performed to confirm the expected change in the electronic density upon the respective unit atoms after complexation.

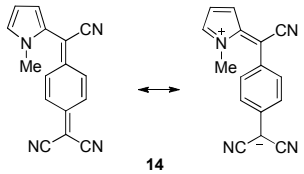

14

X-shaped fully π-conjugated cruciforms where molecules intersect at a central core also exhibit interesting molecular recognition properties. Such properties are engineered through modulation of the FMOs by structural changes leading to spatial separation between donor and acceptor groups. Miljanic et. al.[11]

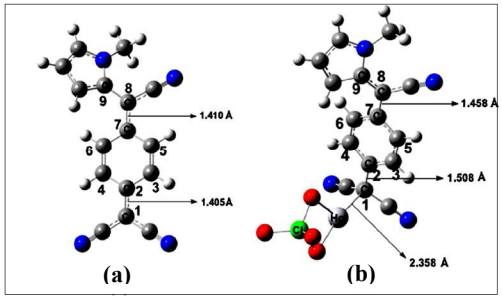

Fig. 15 The energy minimised structures of (a) **14** and (b) **14**: $Hg(ClO_4)_2$ [Reprinted with permission from ref. 10. Copyright 2010 Elsevier].

has explored the influence of electronic effects on the FMOs separation and the associated optical changes in benzobisoxazole based cruciform **15** (Fig.16).

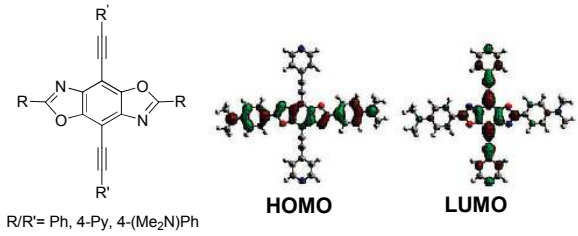

15

Fig. 16 A representative example of spatially separated FMOs. [Reprinted with permission from (ref. 11). Copyright (2011) American Chemical Society].

The hypsochromic and bathochromic shifts in the absorption and emission spectra experienced by the cruciform on protonation, were found to be in good agreement to the preferred stabilisation of FMOs.

A crown ether based derivative **16** responded to Hg^{2+} exhibiting visible ratiometric chromogenic behavior (a gradual decreasing absorbance at 354 nm and increasing absorbance at 408 nm).[12] The bathochromic shift has been attributed to the binding of Hg^{2+} with oxygen atoms in crown ether instead of nitrogen atoms of the azo (-N=N) bonds. A binding mode (Fig. 17), expected to enhance the stability as well as the conjugation of the complex as a consequence of the formation of six rigid five membered rings, which could be responsible for the observed bathochromic shift, has been proposed on the basis of DFT calculations.

Coumarin based derivatives **17** and **18** have been reported[13] to exhibit two photon absorption (TPA) activity in the longer wavelength region, 760-860 nm in the presence of Mg^{2+} and Zn^{2+}, respectively, which has been attributed to increased charge

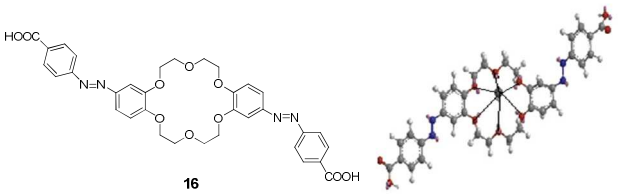

16

Fig. 17 The energy minimised structure of **16**:Hg^{2+} complex [Reprinted with permission from ref. 12. Copyright 2011 Elsevier]

RSC Advances Accepted Manuscript

delocalization on metal binding and was well supported by theoretical calculations. The DFT studies predicted decreased HOMO-LUMO gaps on complexation, facilitating the charge-transfer transition, and the attendant high TPA activity.

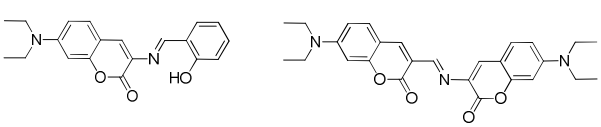

17 18

2.2 Photo Electron transfer (PET) based systems

A coumarin-based compound **19** containing an ionophore with O and N heteroatoms exhibits *"turn-on"* behaviour in the presence of Hg^{2+} ions through the formation of the complex **20** (**19**:Hg^{2+}).[14] A PET process operative from the ionophore to the excited chromophore **19** quenches the emission intensity close to zero. The enhancement of the emission intensity in the presence of Hg^{2+} is attributed to the binding of Hg^{2+} to the ionophore and thereby restricting the PET. The proposed interaction of Hg^{2+} with the ionophore was found to be in good agreement with the DFT calculations which predicted the coordination of Hg^{2+} not only with the heteroatoms of the macrocycle, but also with the sulfur atom of the thioureido linker (Fig. 18).

The azadiene **21** has been developed as a chemosensor for Cu^{2+} and Hg^{2+} exhibiting absorption as well as emission based changes.[15] The non-fluorescent nature of **21** despite having strong fluorophores like pyrene, has been attributed to the result of the PET quenching of the excited state of pyrene by the lone pair of electrons on the nitrogen atom of the bridging group.

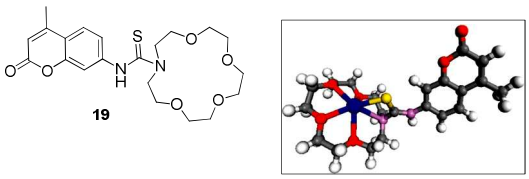

19 20

Fig. **18** The energy minimised structure of complex **20** [Reproduced with permission from ref. 14. Copyright (2010) Royal Society of Chemistry].

Involvement of this lone pair of electron in the complexation with the metal ions, impose restriction on the PET, resulting in enhanced emission intensity. DFT studies supported the formation of a 1:1 stoichiometric complex of **21** with Cu^{2+}.

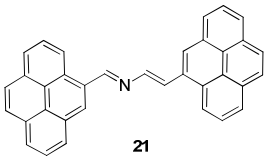

21

The best optimized structure of **21**:$Cu(OTf)_2$ complex, exhibited hexacoordination around the Cu^{2+} ion (Fig. 19), one site being occupied by azadiene N atom (d_{N-Cu} = 2.037), four sites by OTf oxygen atoms (two equatorial d_{O-Cu} = 2.024 and 2.115 Å, two axial d_{O-Cu} = 2.534 and 2.619 Å) and a weak contact with one of the carbon atom of pyrenyl group (d_{C-Cu} = 2.350 Å).

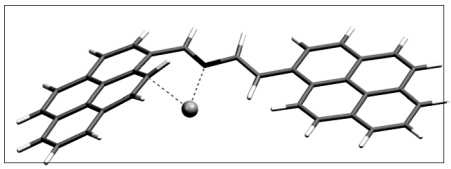

Fig. 19 The energy minimised structure of **21**: Cu^{2+} [Reprinted with permission from ref. 15. Copyright 2010 Elsevier].

Similar fluorescence enhancement and the bathochromic shift in the absorption peak were exhibited by the pyrene-thiourea based derivative **22** in the presence of Cu^{2+} and Hg^{2+}.[16] Through the mechanism of PET quenching as proposed for **21**, a geometry **22**:Cu^{2+} (Fig. 20) has been proposed in support of the observed fluorescence "*on-off*" behaviour (Fig. 21).

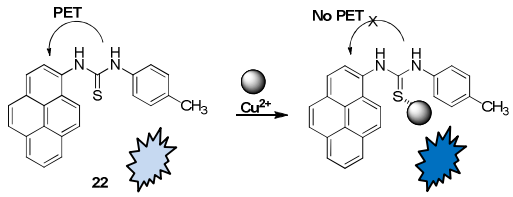

Fig. 20 Fluorescence "*on-off*" behaviour of **22** upon recognition of Cu^{2+}.

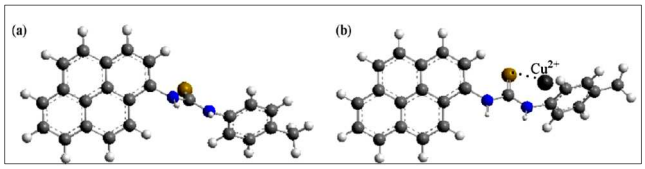

(a) **(b)**

Fig. 21 The energy minimised structure of (a) **22** and (b) **22**:Cu^{2+} complex [Reprinted with permission from ref. 16. Copyright 2010 Elsevier].

A sugar-aza-crown ether based fluorescent compound **23** recognizes $Cu^{2+}$and Hg^{2+}, selectively.[17] The observed fluorescence intensity enhancement has been attributed to the PET that occurs upon complexation of the nitrogen atoms by the metal ions. The suggested complexation mode was further supported by the DFT studies. The most stable optimized structure obtained for Hg^{2+} indicates the presence of Hg^{2+} in the coordination centre of **23**, surrounded by two nitrogen and two oxygen atoms from the linker and the ribosyl unit, respectively, with the average bond lengths of 2.52 Å (Hg-N) and 2.53 Å (Hg-O) (Fig. 22).

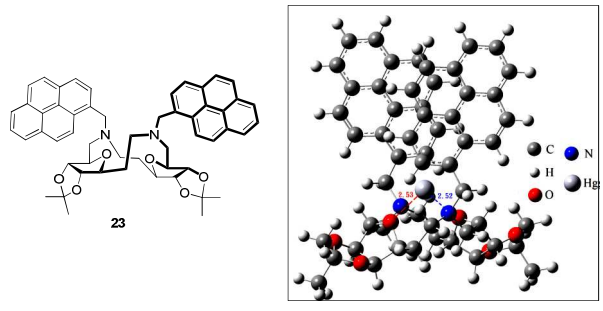

23

Fig. 22 Energy minimised structures of **23**:Hg^{2+} [Reprinted with permission from ref. 17. Copyright 2011 Elsevier].

RSC Advances Accepted Manuscript

This journal is © The Royal Society of Chemistry [year]

A benzoimidazole based derivative **24** was found to be selective for Zn^{2+}.[18] Thebathochromically shifted absorption and fluorescence enhanced behaviour exhibited by **24** in the presence of Zn^{2+} has been assigned to the change in dihedral angle between aryl and the benzoimidazole plane of **24**, influencing PET from tertiary amine nitrogen atom to the fluorophore in the excited state of **24**, on the basis of DFT calculations. The dihedral angle (30.63°) between the above said two planes, noted in the best optimized structure of free **24** (Fig. 23), has been suggested to cause photo-induced electron as well as photo-induced energy transfer, leading to weak fluorescence. However, the coordination of Zn^{2+} to the bipicolyl amine site reduced the dihedral angle (19.63°) owing to the coplanarity, thus causing a red shift in the absorption and emission bands. As a result of the change in dihedral angle, the PET process gets restricted which results in the observed emission enhancement.

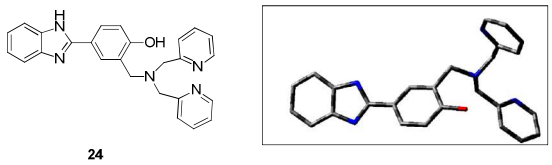

Fig. 23 Energy minimised structures of **24**:Zn^{2+} complex depicting the dihedral angle [Reprinted with permission from ref. 18. Copyright 2012 Elsevier].

An otherwise non-fluorescent rosamine derivative **25** having [15]aneNO$_2$S$_2$ as a binding unit exhibits fluorescence enhancement in the presence of Ag^+ and Hg^{2+}.[19] The non-fluorescent nature of **25** has been assigned to the electron transfer from the HOMO of [15]aneNO$_2$S$_2$ to the HOMO of the of the excited fluorophore **25** which is lower in energy (Fig. 24a). However, on binding with the metal ions, the HOMO of [15]aneNO$_2$S$_2$ gets more stabilized, thereby restricting the electron transfer to the HOMO of the fluorophore at higher energy, thus leading to the enhanced fluorescence intensity (Fig. 24b).

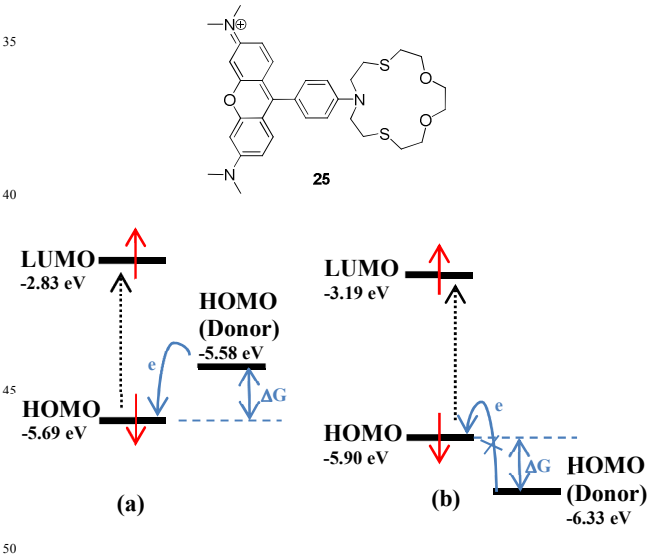

Fig. 24 The comparative energy levels of (a) **25** and (b) **25**:Ag^+, depicting the mechanism of fluorescence enhancement in **25**:Ag^+ complex.

Interestingly, the fluorescence intensity enhancement effect of both the metal ions was entirely opposite in acetonitrile and water. This contrasting behaviour was also well supported by the DFT calculations. In acetonitrile, the HOMO energy gap between [15]aneNO$_2$S$_2$-Ag^+ and the fluorophore was predicted to be much less (-0.48 eV) as compared to [15]aneNO$_2$S$_2$-Hg^{2+} (-0.71 eV). Thus, the extensive PET inhibition by Hg^{2+} induces much more fluorescence enhancement than Ag^+. On the other hand, in water, the HOMO energy gap between [15]aneNO$_2$S$_2$-Ag^+ and the fluorophore (-0.43 eV) was predicted to be much more than that between [15]aneNO$_2$S$_2$-Hg^{2+} and fluorophore (-0.01 eV). Thus, Ag^+ could induce more fluorescence enhancement in water (Fig. 25).

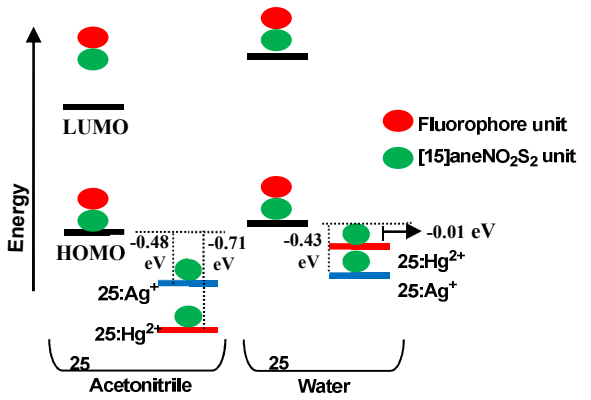

Fig. 25 Comparative energy levels of **25**, **25**:Ag^+ and **25**:Hg^{2+} complexes in acetonitrile and water.

2.3 Binding mode based systems

Imidazole-annelated ferrocene derivatives **26** and **27** have been developed as multichannel chemical probes for the Pb^{2+} ions.[20a] The sensing event is accomplished via chromogenic (bathochromically shifted absorption band), fluorescent (chelation enhanced fluorescence, CHEF) and redox (anodically shifted redox peak) changes, in both **26** and **27** in the presence of Pb^{2+} ions. The derivatives **28** and **29** also exhibited a similar behaviour. The associated color changes are shown in Fig. 26. The reversibility of the sensing event upon addition of ethylenediamine suggested binding of the metal ion to the receptor through weak interactions. This hypothesis was, in fact, supported by the Truhlar's hybrid metafunctional MPW1B 95,[20b-d] DFT calculations, which are useful for studying the systems with non-covalent interactions.

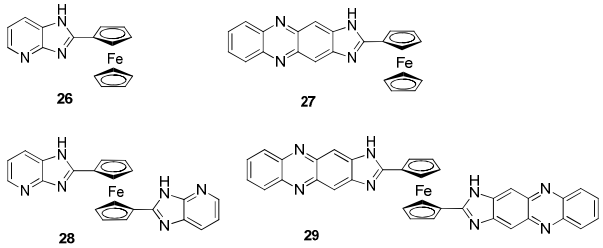

RSC Advances Accepted Manuscript

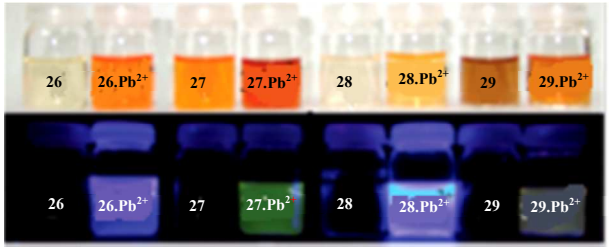

Fig. 26 Color changes observed for **26-29** in the presence of Pb^{2+} (top) absorption and (bottom) emission [Reproduced with permission from (ref. 20a). Copyright (2009) American Chemical Society].

The calculations predicted binding of both the pyridine as well as imidazole N atoms of **26** with Pb^{2+} ($d_{Pb\text{-}N}$ = 2.565 Å and $d_{Pb\text{-}N}$ = 3.037 Å, respectively) (Fig. 27), leading to the formation of **26**:$Pb(ClO_4)_2(CH_3CN)_2$ complex. However, the receptor **27**, which lacks an additional pair of nitrogen atom, could not presumably act as a bidentate ligand and led to a more favourable $(\mathbf{27})_2$:Pb^{2+} stoichiometric complex. Further, the significant bathochromic shift observed in the absorption spectrum, as a consequence of binding led to the naked eye color change. The proposed binding model was in good agreement with the TD-DFT calculations performed for **26**: Pb^{2+}. The main low energy absorption band in **26** is contributed by a HOMO/HOMO-1→LUMO transition (Fig. 28).

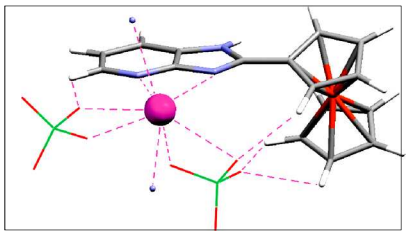

Fig. 27 Calculated structure for **26**:$Pb(ClO_4)_2(CH_3CN)_2$ complex. Only nitrogen atom of CH_3CN is shown [Reprinted with permission from (ref. 20a). Copyright (2009) American Chemical Society].

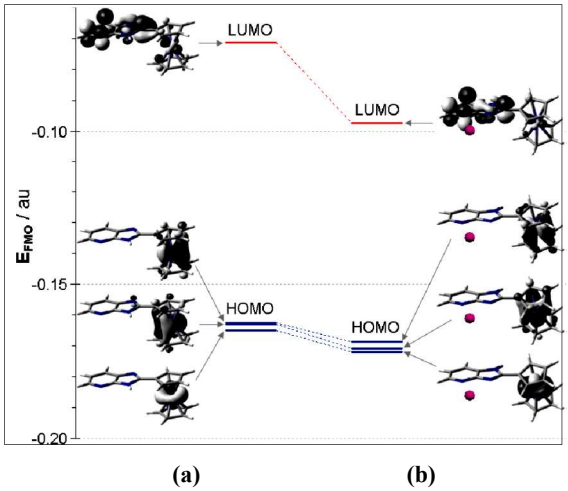

Fig. 28 Calculated molecular orbital diagram for (a) **26** and (b) **26**:$Pb(ClO_4)_2(CH_3CN)_2$ complex [Reprinted with permission from (ref. 20a). Copyright (2009) American Chemical Society].

Although, both HOMO and LUMO of the free **26** get stabilized upon complexation with Pb^{2+}, the LUMO experiences a significant stabilization with respect to HOMOs, which is responsible for the observed bathochromic shift.

A ferrocene-azaquinoxaline based dyad **30** detects Hg^{2+}, Pb^{2+} and Zn^{2+} ions via three different channels exhibiting identical sensing properties towards each of the three metal ions as deduced from the anodically shifted redox peaks, as well as high florescence enhancement and visible colorimetric change.[21] However, a more

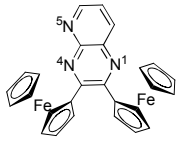

30

pronounced color change of the ligand was observed in case of complexation with Hg^{2+} ions. This has been well supported by the binding behaviour of **30** towards different metal ions predicted on the basis of DFT calculations (Fig. 29). In case of Zn^{2+}, the most stable complex stoichiometry $(\mathbf{30})_2$:$Zn(ClO_4)_2$ indicates $^{4,5}N$ coordination in one of the ligands ($d^5_{N\text{-}Zn}$ = 2.198 Å, $d^4_{N\text{-}Zn}$ = 2.414 Å, but almost exclusive ^5N binding mode for the other ligand ($d^5_{N\text{-}Zn}$ = 2.127 Å, $d^4_{N\text{-}Zn}$ = 2.877 Å), presumably due to steric crowding around the relatively small (Zn^{2+}) metal ion, thus indicating the presence of two different heterocyclic ligands (Fig. 29a). In contrast to this, the larger Pb^{2+} cation in $(\mathbf{30})_2$:$Pb(ClO_4)_2$ allows approximation of both the ligands exhibiting $^{4,5}N$ binding mechanism ($d^5_{N\text{-}Pb}$ = 2.546 and 2.864 Å, $d^4_{N\text{-}Pb}$ = 2.769 and 2.747 Å), thus indicating the presence of two very similar heterocyclic ligands (Fig. 29b). In case of Hg^{2+}, the structure of the most stable complex is **30**:$Hg(ClO_4)_2$ exhibiting typical N-Hg bond distances ($d^5_{N\text{-}Hg}$ = 2.491 Å, $d^4_{N\text{-}Hg}$ = 2.518 Å) (Fig. 29c). However, when the terminal ^1N atom in the 1:1 optimised structure was also made to involve in binding with the identical molecule, formation of a 2:2 stoichiometric $(\mathbf{30})_2$:$(Hg(ClO_4)_2)_2$ as a stable complex was revealed (Fig. 29d).

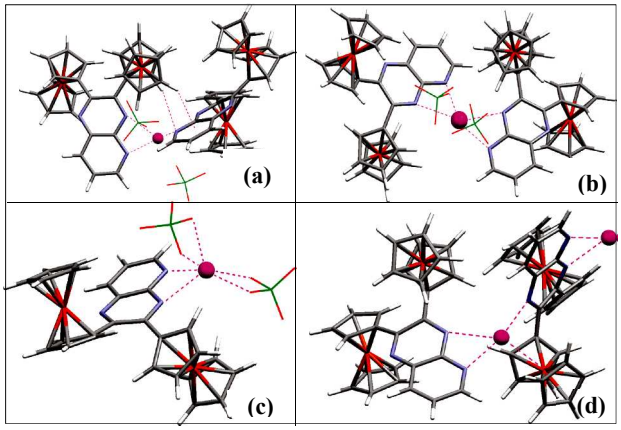

Fig. 29 Calculated structures for (a) $(\mathbf{30})_2$:$Zn(ClO_4)_2$, (b) $(\mathbf{30})_2$:$Pb(ClO_4)_2$, (c) **30**:$Hg(ClO_4)_2$ and (d) $(\mathbf{30})_2$:$[Hg(ClO_4)_2]_2$ [Reprinted with permission from (ref. 21). Copyright (2009) American Chemical Society].

The prominent feature of this binding model is the interaction of the internal Hg^{2+} cation with the adjacent ferrocenyl iron atom, which was not observed in the complexes of the other two metal ions, and thus this additional binding mode has been held energy

RSC Advances Accepted Manuscript

This journal is © The Royal Society of Chemistry [year]

responsible for the pronounced color change. The predicted MO level diagram for **30** shows that the low energy optical transition should involve the HOMO→LUMO transition, HOMO being located on ferrocene and π^*-type LUMO on the heterocyclic moieties and that this energy difference decreases subsequent to complexation. This decrease has been predicted to be more pronounced for the 2:2 complex (Table 2).

Table 2 Predicted optical transitions for **30** and its complexes with Zn^{2+}, Pb^{2+} and Hg^{2+}.

S. No.	Compound	Transition	λ_{max}
1.	**30**	HOMO-LUMO π^*	399 nm
2.	(**30**)$_2$:$Zn(ClO_4)_2$	HOMO-LUMO π_1^*, π_2^*	523 nm
3.	(**30**)$_2$:$Pb(ClO_4)_2$	HOMO-LUMO π_1^*/ π_2^* π_2^*/ π_1^*	460 nm
4.	**30**:$Hg(ClO_4)_2$	HOMO-LUMO π^*	499 nm
5.	(**30**)$_2$:$[Hg(ClO_4)_2]_2$	HOMO-LUMO π_1^*	568 nm

A series of pyrene derivatives **31-33** was synthesized and evaluated for their behaviour towards recognition of cations.[22] Out of these, only **31** could yield the significant results.

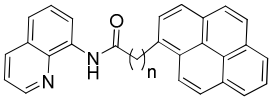

31: n = 0
32: n = 1
33: n = 3

It exhibited a strong static excimer emission in the presence of Cu^{2+} indicating the formation of a dimer of **31**. The recognition of Cu^{2+} ion led to self-assembled pyrenyl excimer formation which has additionally been rationalized by the DFT calculations. The best optimized structures of dimeric **31-33** have suggested the contribution of hydrogen bonding in the self-assembling of all the three pyrene derivatives. The binding energies have been calculated as 12.0, 19.4 and 22.4 kcal/mole for **31**, **32** and **33**, respectively (Fig. 30). Due to high binding energies, sometimes it is thermodynamically less favorable for a guest species to disturb the stable electrostatic interactions between the two monomer units. In line with this hypothesis, only **31** having less binding energy, of the three, led to recognition of Cu^{2+}. Further the lowest energy structure of **31**:Cu^{2+} complex (Fig. 31) indicated the participation of the amide oxygen next to the pyrene in the recognition event which was also supported by natural population analysis (NPA) suggestive of the distinct electron density change in oxygen upon Cu^{2+} ion complexation. The strong fluorescence excimer band for **31**:Cu^{2+} complex was rationalized by TD-DFT calculations suggesting the HOMO to LUMO excitations from one pyrene to the other facing pyrene (Py-Py* interaction) responsible for the observed behaviour.

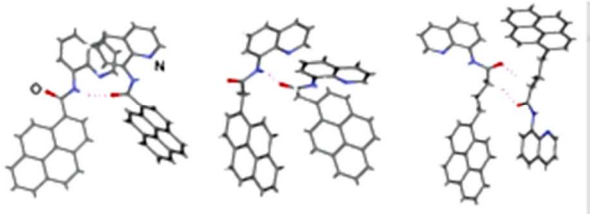

(a) **(b)** **(c)**

Fig. 30 Global minima structures for the dimers of (a) **31**, (b) **32** and (c) **33**. Hydrogen bonds are shown as dotted lines [Reprinted with permission from (ref. 22). Copyright (2009) American Chemical Society].

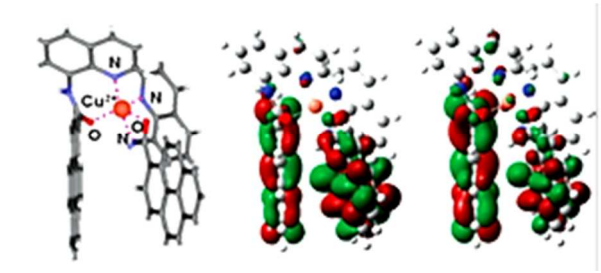

(a) **(b)** **(c)**

Fig. 31 (a) Lowest energy structure for**31**:Cu^{2+}, (b) HOMO of **31**:Cu^{2+} and (c) LUMO of **31**:Cu^{2+} complex [Reprinted with permission from (ref. 22). Copyright (2009) American Chemical Society].

Coumarin based fluorescent compound **34** exhibits "*turn-off*" response upon recognition of Cu^{2+}.[23] The proposed complexation mode of **34** with Cu^{2+} (Fig. 32) was well supported by DFT calculations. The energy minimized structure indicates that Cu^{2+} ions occupy the central coordination site of **34** and the whole molecule attains a planar structure with the Cu-N bond length of 2.00 Å, and the Cu-O bond length of 2.03 and 1.95 Å (for Cu-coumarin and Cu-benzoylhydrazine, respectively).

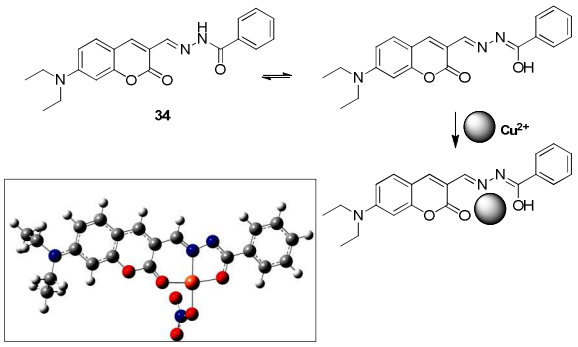

34

Fig. 32 Formation and energy minimized structure of **34**:$Cu(NO_3)_2$ [Reproduced with permission from ref. 23. Copyright (2011) Royal Society of Chemistry].

The effect of structure modifications on the optical properties in π-conjugated systems has been demonstrated in α-monoacylated, α, α'- and α, β-diacylated dipyrrins (**35-37**), respectively, which are fluorescence "*turn-on*" probes for Zn^{2+} ions.[24] The observed bathochromic shifts in emission wavelengths in the series **35** to **37**, upon interaction with Zn^{2+} were found to be in good agreement with the predicted HOMO-LUMO energy gaps (Fig. 33).

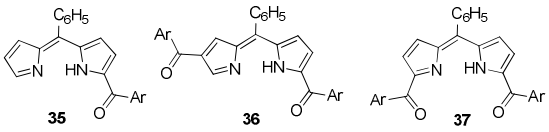

35 **36** **37**

The triad **38** detects Hg^{2+} via electrochemical, spectral and optical transduction channels.[25] The corresponding experimental responses such as, positive shift in potential, bathochromic shift of the absorption bands accompanied by a naked-eye color change, exhibited by **38** in the presence of Hg^{2+} has been attributed to the grabing of Hg^{2+} by both side-arms of the receptor

RSC Advances Accepted Manuscript

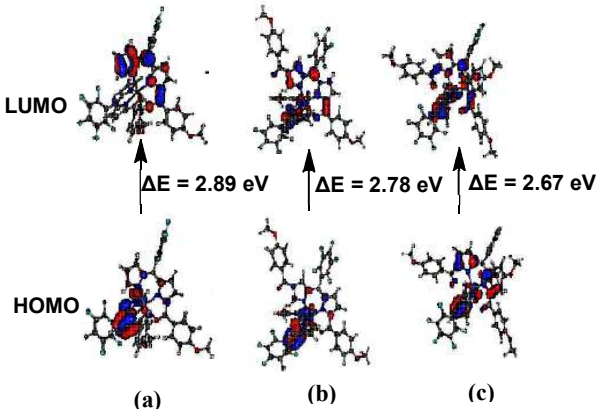

Fig. 33 Comparative energy level diagram of (a) Zn(**35**)$_2$, (b) Zn(**36**)$_2$ and (c) Zn(**37**)$_2$.[Reprinted with permission from (ref. 24). Copyright (2013) American Chemical Society].

by the action of both azadiene N atoms as predicted by DFT-based quantum chemical calculations ($d_{N\text{-}Hg}$ = 2.201Å, N-Hg-N 151.5°). The energy minimised structure of the complex **38**:Hg^{2+} exhibits C_2-symmetry as sown in Fig. 34.

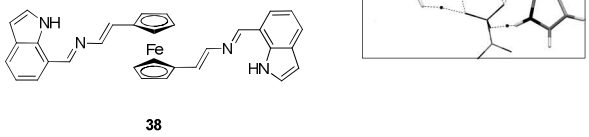

Fig. 34 The energy minimised structure of **38**:Hg^{2+} [Reproduced with permission from ref. 25. Copyright (2009) Royal Society of Chemistry].

3. Anion recognition

3.1 Reaction based systems

A spiropyran derivative **39** behaves as a selective and sensitive CN^- receptor in aqueous media under UV irradiation utilizing the nucleophilicity of the CN^-.[26] The observed hypsochromic shift in the absorption band of **39** upon cyanide addition is attributed to the addition of CN^- to the spirocarbon of the merocyanine (MC) form of **39** (formed upon UV irradiation) producing a spirocyclic-opened species (**39**:CN^-) (Fig. 35). The observed hypsochromic shift is in good agreement with the *ab initio* calculations, predicting that the lowest singlet electronic transitions of both **39** (MC) and **39**:CN^- are mainly contributed by a HOMO-LUMO transition having $\pi \rightarrow \pi^*$ character. The predicted less HOMO-LUMO energy difference (Fig. 35, inset) in **39** (MC) (2.67 eV) as compared to **39**:CN^- (3.29 eV), has been assigned as the probable reason for the observed chromogenic response.

The receptors bearing salicylaldehyde hydrazone functionality **40** and **41** detect CN^- from aqueous solution via fluorogenic and chromogenic transduction channels, respectively, utilizing the nucleophilicity of CN^-.[27] The nucleophilic attack of CN^- at imine functionality of **40** and **41** leads to the formation of 1:1 adduct of CN^- with both the receptors, however, with revived fluorescence in case of non-fluorescent **40**, and a visual color change in **41**.

The DFT calculations performed on **40** predicted a dispersed HOMO electron density over the whole molecule which gets partially dispersed from the 4-(N,N- dimethylamino)benzamide

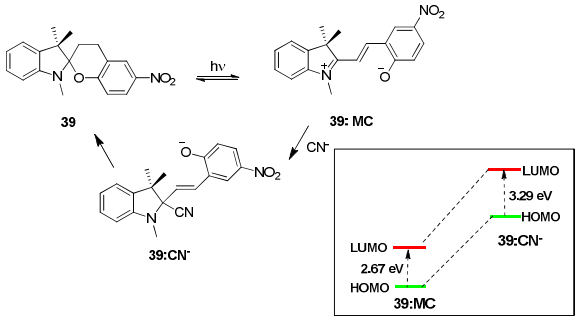

Fig. 35 Recognition of CN- through photo-induced nucleophilic substitution to spiropyran 39 (inset: HOMO-LUMO energy changes).

fluorophore to the salicylaldehyde hydrazone moiety upon excitation leading to the weak fluorescence. However, in the CN^- adduct, HOMO-LUMO excitation completely moves the electron density distribution from phenoxide anion to the fluorophore (Fig. 36) resulting in the decay of the excited state, thus reviving the fluorescence.

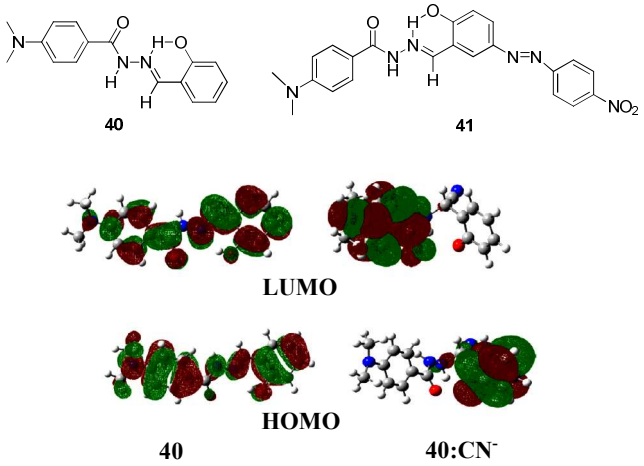

Fig. 36 Comparative electron density distribution in HOMO and LUMO energy levels of **40** and **40**:CN^- [Reprinted with permission from ref. 27. Copyright 2009 Elsevier].

The cationic boron compounds **42** and **43** detect F^- in a mixture of $H_2O/CHCl_3$.[28] The sensing process is accomplished by the formation of the Zwitterion fluoroborates (Fig. 37), which are characterized by bathochromically shifted absorption band (ICT in nature) in comparison to **42** and **43**. The bathochromic shift is attributed to the decreased HOMO-LUMO gap, localized on the mesityl (Mes) and the pyridinium units, respectively.

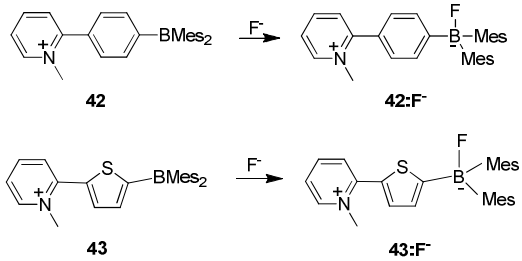

Fig. 37 Detection of F^- by cationic boronic derivatives.

RSC Advances Accepted Manuscript

This journal is © The Royal Society of Chemistry [year]

The N-benzamido-bisthiourea derivative **44** undergoes interesting changes in its optical behaviour on detecting F^- ion.[29] A concentration dependent hypsochromic shift followed by bathochromic shift in the absorption band of **44** was observed upon gradual addition of F^- indicating the presence of three different species:**44**, **44**:F^- and **44**:$(F^-)_2$, in equilibrium. Similarly, emission spectral studies exhibit initial fluorescence quenching without any spectral shift followed by the appearance of a new bathochromically shifted emission band. On the basis of these observations, it was proposed that at lower concentration, the interaction of the F^- is through hydrogen-bonding with the bisthiourea moiety (responsible for the hypsochromic shift) corresponding to the formation of **44**:F^- species, which is then followed by deprotonation of thiourea NH at higher concentration of F^- (responsible for bathochromically shifted absorption alongwith emission quenching), corresponding to the formation of **44**: $(F^-)_2$ species (Fig. 38).

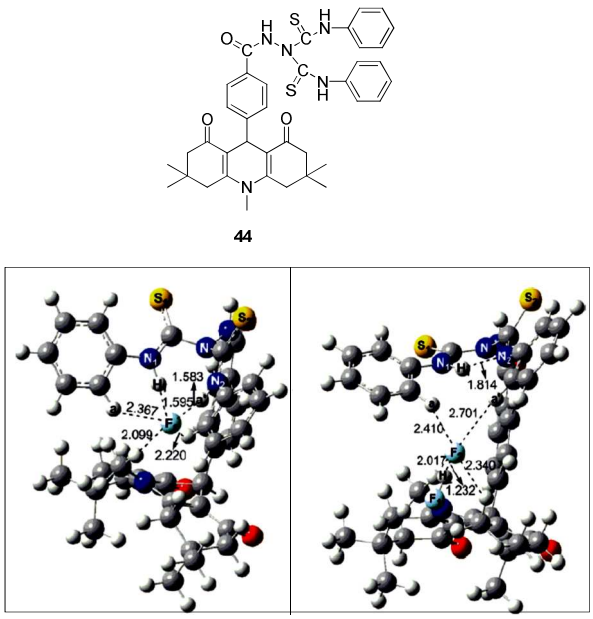

Fig. 38 Energy minimised structures of **44**:F^- and **44**:$(F^-)_2$ [Reproduced with permission from ref. 29. Copyright (2010) Royal Society of Chemistry].

The DFT calculations predicted that for all the three species, while HOMO is localized on the sulfur atom of thiourea and is nonbonding in nature, the LUMO is π* in nature and is localized on the second thiourea group of **44**. The contribution to the absorption band of **44** is mainly from HOMO→LUMO transition (S_1 state). In **44**:F^-, the thiourea attains LUMO+1 orbital, thus the hypsochromically shifted band is the result of HOMO→LUMO+1 transition (S_1 state). In **44**: $(F^-)_2$, the energy of HOMO→LUMO (S_1 state), becomes lower, thus accounts for the new bathochromically shifted absorption band (Fig. 39). The formation of this new state is responsible for the new emission band. The ICT band of benzoxadiazole derivative **45**, resulting from the ICT from N,N-dimethylamine group acting as donor to the dicyanovinyl group acting as acceptor, gets hypsochromically shifted in the presence of CN^-.[30]

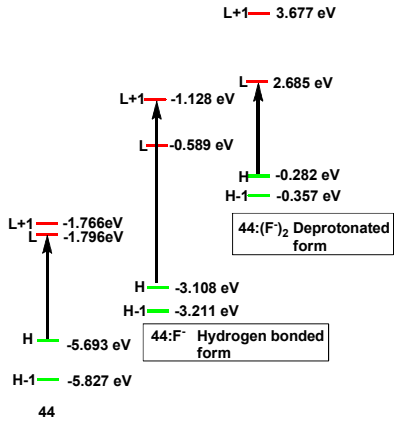

Fig. 39 Comparative energy levels of **44**, **44**:F^- and **44:** $(F^-)_2$.

This shift has been attributed to the inhibited ICT, as a result of addition of CN^- to the α-position of the dicyanovinyl group reducing its electron accepting ability. The optimized structure of **45** and **45**:CN^- indicates significant

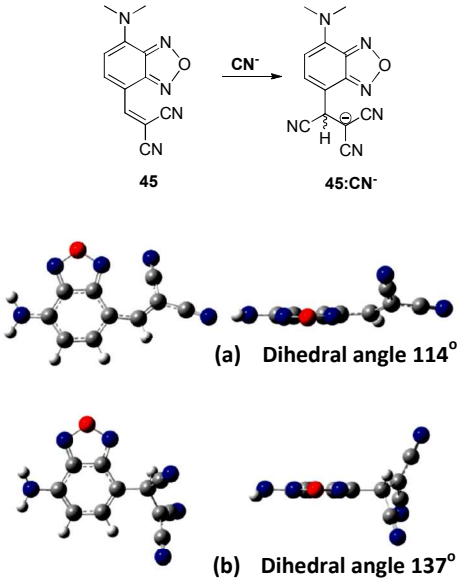

Fig. 40 Energy minimised structures of (a) **45** and (b) **45**:CN^- [Reprinted with permission from (ref. 30). Copyright (2011) American Chemical Society].

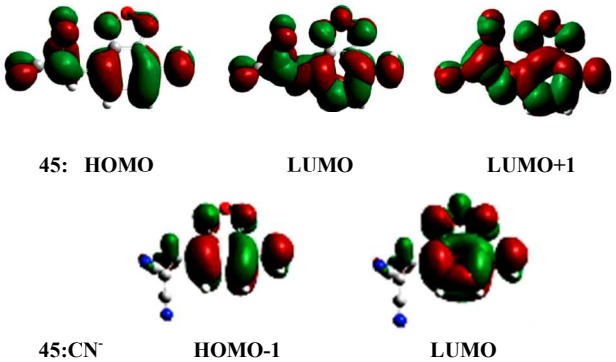

Fig. 41 The electron density distribution in the various energy levels of **45** and **45**:CN^- [Reprinted with permission from (ref. 30). Copyright (2011) American Chemical Society].

RSC Advances Accepted Manuscript

difference in the π-conjunction with respect to change of conjugated bridge (-C=C-) and dihedral angle of 114° between the benzoxadiazole group and dicyano group in **45** to a saturated bridge (-C-C-) with dihedral angle of 137° in **45**:CN^- (Fig. 40). It was further corroborated by the calculated HOMOs and LUMOs of **45** and **45**:CN^-. From the locations of LUMO in **45** (Fig. 41), it is clear that the ICT takes place through the conjugated bridge between the benzoxadiazole and dicyano groups, whereas in **45**:CN^-, it is restricted.

The "*turn-on*" fluorescence chemosensing behaviour of 8-formyl-7-hydroxycoumarin **46** in the presence of CN^- was investigated and authenticated to a large extent by TD-DFT studies in the ground and the first excited states of both the **46** and its CN^- addition product **47**.[31] On the basis of these studies, it was proposed that in the first singlet excited state (S_1), the phenolic proton of **46** transfers to the neighbouring formyl group along with the intramolecular hydrogen bond, whereas **47** observes proton transfer process in the ground state, and consequently has the similar structure in the first excited state. This accounts for the experimentally observed strong fluorescence during the sensing event. Further, the molecular orbital analysis also predicts an S_0-S_1 transition at a lower energy in **47** as compared to **46**. From the shapes of the FMOs involved in **46** and **47**, it can be seen that while the HOMOs of both **46** and **47** are located on the coumarin ring, the LUMO orbitals are additionally spread over the 8-formyl substituent also in **46**, whereas, in **47** these are located mainly on the coumarin unit (Fig. 42). On the basis of this, it was concluded that S_1 states of both are ICT states operative in reverse directions. Prior to this, similar type of studies were reported on the sensing mechanism of a F^- chemosensor, phenyl-1*H*-anthra(1,2-d)imidazole-6,11-dione.[32]

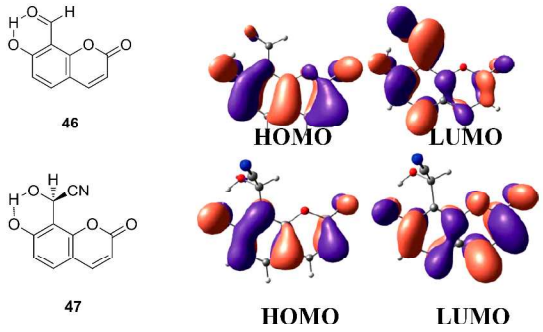

Fig. 42 Electron density distribution in the HOMO and LUMO energy levels of **46** and **47** [Reproduced with permission from (ref. 31). Copyright (2010) Wiley-VCH].

A unique anion to cation relay recognition concept has been established in the sensing of F^- followed by Cu^{2+} ions (Fig. 43).[33] The proposed fluorescence "*turn-on*" behaviour of **48** in the presence of F^-, based upon formation of a specific cyclisation product **49** and "*turn-off*" behaviour of the *in-situ* formed **49** in the presence of Cu^{2+} via formation of a 1:1 complex **50** (Fig 43), has been well supported by DFT calculations. The decrease in dihedral angle in **49** in comparison to **48** suggested the enhanced planarity and subsequent delocalised π bonds which enhanced the fluorescence emission. Also, the identical energy gaps between HOMOs and LUMOs of **48** and **49** are in good agreement with the observed unperturbed absorption spectral pattern. On the other hand, the best optimised structure of the Cu^{2+} complex **50** of *in situ* formed complex **49**, suggested the binding of Cu^{2+} to nitrogen atoms of the imino and benzothiazole groups. A LMCT, as predicted by the localisation of HOMO-2 and LUMO in **50**, may lead to the observed "*turn-off*" fluorescent behaviour and bathochromic shift in the absorption spectrum of **3** (Fig. 44).

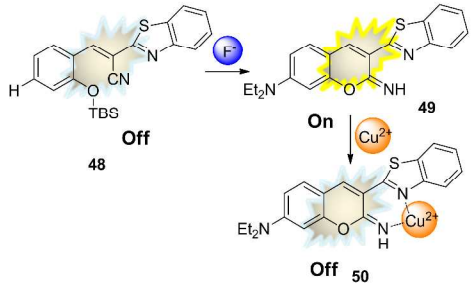

Fig. 43 Anion to cation *Relay* recognition mechanism.

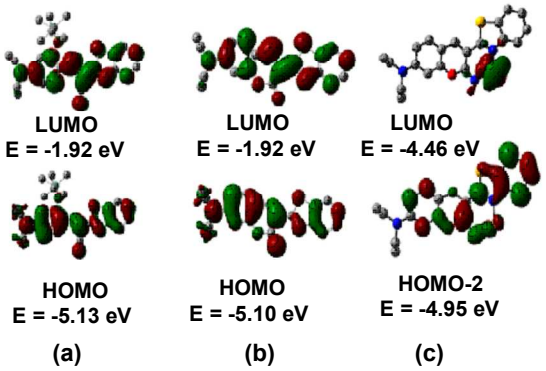

Fig. 44 HOMO and LUMO energy levels of (a) **48**, (b) **49** and (c) **50.** [Reprinted with permission from (ref. 33). Copyright (2011) American Chemical Society].

3.2 Displacement/elimination reaction based systems

A supramolecular ensemble **51** resulted from the complexation of chromenolate anion with bis-pyridinium calix[4] pyrrole, detects pyrophosphate over other competing anions including even phosphate anions.[34] The sensing event takes the advantage of the fluorescence dye displacement mechanism releasing the fluorescent chemoenolate anion and trapping pyrophosphate anion by **51**. The supramolecular trapping is facilitated by the combined benefit of electrostatic, anion-π and hydrogen bond interactions.

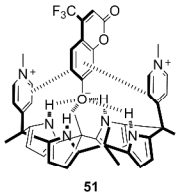

The pyrene derivative **52** exhibits a hypsochromic shift in its absorption as well as emission spectra on detecting F^- ion over

RSC Advances Accepted Manuscript

This journal is © The Royal Society of Chemistry [year]

the other anions.[35] The mechanism involving elimination of the trimethylsilyl substituent by the F^- ion has been proposed to be responsible for the sensing event. DFT calculations have suggested that on elimination of trimethylsilyl group, the HOMO-LUMO energy difference increases, which is responsible for the observed spectral as well as visual changes (Fig. 45).

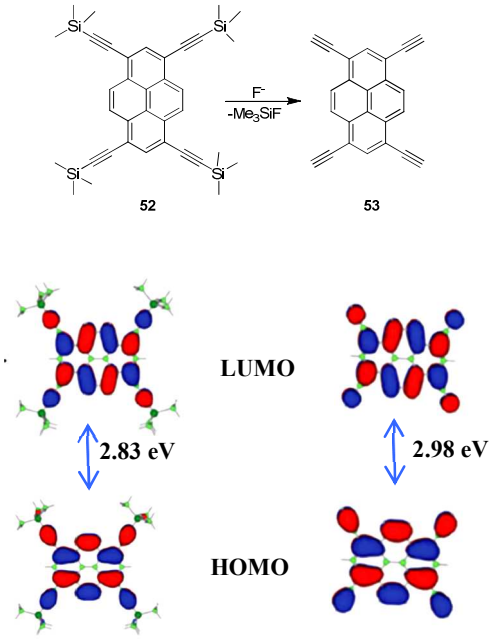

Fig. 45 Comparative energy difference between the HOMOs and LIMOs of **52** and **53** [Reproduced with permission from ref. 35. Copyright (2011) Royal Society of Chemistry].

4. Neutral analyte recognition

4.1 Reaction/redox reaction based systems

The absorption as well as emission bands of a diketpyrrolopyrrole **54** undergo hypsochromic shifts in the presence of cysteine.[36] The absorption band at 659 nm was suggested to be an ICT band on the basis of the localization of the HOMO and LUMO on the diketpyrrolopyrrole (fluorophore) core and malononitrile moiety, respectively, in the ground state as predicted by DFT calculations. On the other hand, emission transition at 666 nm has

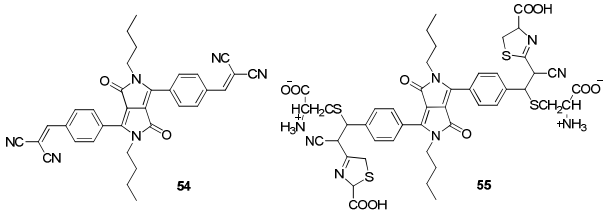

been assigned as a conformation transformation process with the excited state LUMO energy level lower than that of the ground state level and the excited state HOMO energy level higher than that of the ground state, thereby decreasing the energy required for HOMO-LUMO transition in the excited state, as depicted in Fig. 46. However, in **55**, the adduct of **54** and cysteine, the magnitude of ICT transition was predicted to be decreased in the ground state as a result of the more localization of ICT transition (S_0 to S_1) on the diketpyrrolopyrrole chromophore. Like **54**, the emission transition in **55** has also been assigned as conformation transformation process, but with the HOMO-LUMO energy difference greater than the free **54** in the excited state. These results are in good agreement with the observed hypsochromic shift in the absorption and emission bands of **54** in the presence of cysteine.

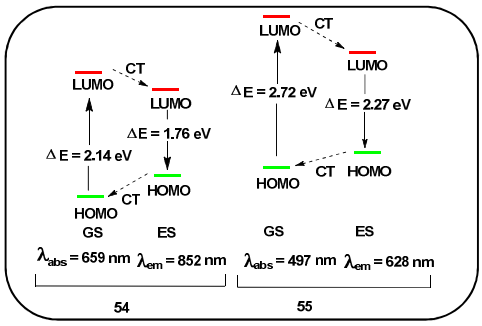

Fig. 46 The predicted energies of the HOMOs and LUMOs of **54** and its cysteine adduct **55**. GS-ground state, ES-excited state, CT-conformational transition.

A pyrene based sensor **56** (Fig. 47) exhibits a significant colorimetric change from light yellow to pink as well as enhanced fluorescence in the presence of lysine over a number of amino acids.[37] The sensing protocol has been ascribed to the formation of a Schiff base **57**. The DFT calculations revealed the formation of a stacked dimer of **57** (Fig. 47b), proposed to be stabilized by water mediated intramolecular hydrogen bonding between C=N, OH and lysine COOH groups as depicted in Fig. 47c.

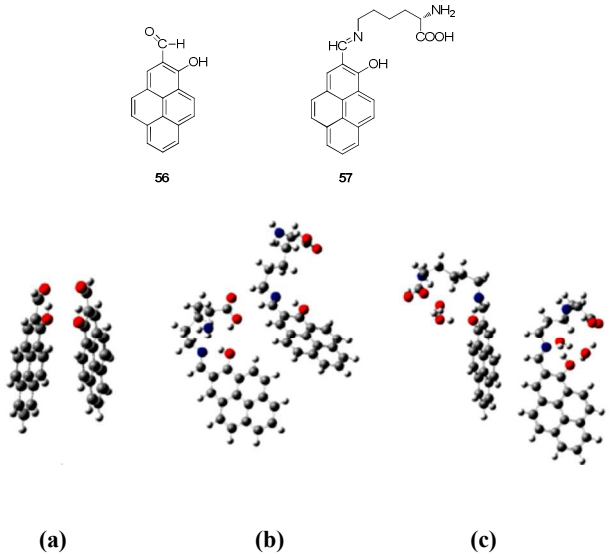

Fig. 47 Energy minimised structures of (a) **56,** (b) dimeric form of **57** and (c) dimeric form of **57**-$(H_2O)_2$ [Reproduced with permission from ref. **37**. Copyright (2011) Royal Society of Chemistry].

The hybrid material Z30-SQ **58** obtained by the inclusion of squaraine dye **59** in the supercages of Zeolite Y with a

RSC Advances Accepted Manuscript

SiO_2/Al_2O_3 ratio of 30 (Z30) (Fig. 48), was found to be sensitive towards the presence of volatile propylamine and propylthiol over other volatile organic compounds like acetone, ethanol, dichloromethane, hexane, acetonitrile, ethyl acetate, ethyl ether and acetic acid.[38] The sensing mechanism has been ascribed to the reaction of **59** with thiol and the amine compounds resulting in the spectral and visual changes. Interestingly, the reaction with thiol was partially reversible whereas with amine was irreversible

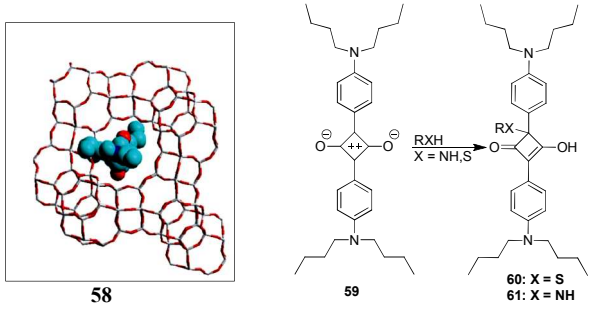

Fig. 48 Recognition of *n*-propylamine and *n*-propylthiol by supercaged squarine **59** [Reproduced with permission from ref. 38. Copyright (2011) Royal Society of Chemistry].

pointing towards the weaker thiol adduct **60** as compared to amine adduct **61**. It was further corroborated by the optimized geometries of these two adducts, predicting the S-C and N-C bond lengths of 1.90 and 1.50 Å, respectively (Fig. 49a). However, when geometry optimization was performed with acetone or propanol, no reaction was found (distance between oxygen atom of acetone/ propanol and **59** was found to increase to 4Å) (Fig. 49b).

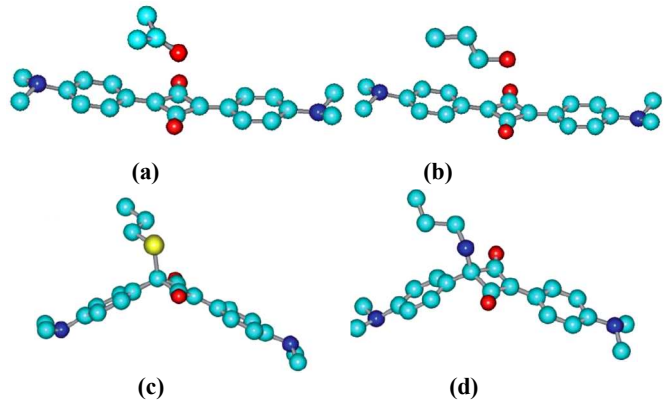

Fig. 49 Energy minimised structures of **59** (a) with acetone, (b) with *n*-propanol, (c) **60** and (d) **61**. [Reproduced with permission from ref. 38. Copyright (2011) Royal Society of Chemistry].

A dimethylamino-1,4-benzoxazin-2-one based derivative **62** detects cysteine and homocysteine via chemodosimetric action forming the product **63**, with enhanced fluorescence intensity and hypsochromically shifted absorption band.[39] The main absorption band of **62**, possessing electron donor amino group and electron withdrawing carbonyl group has been assigned an ICT nature with contribution from HOMO-LUMO transition (3.35 eV). Subsequent to the formation of **63**, the ICT gets perturbed leading to the enhanced energy difference between HOMO and LUMO (3.39 eV) which is responsible for the experimentally observed hypsochromic shift.

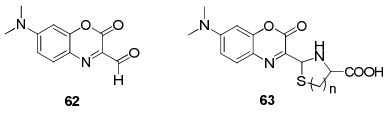

The dialdehyde substituted borondipyromethane (BODIPY) dye **64**, being highly electron deficient and prone to facile reductions, exhibited pH dependent *"on/off"* fluorescence and thus could be labelled as pH sensors.[40] The electron deficiency was also predicted by DFT calculations performed on both the di-substituted and unsubstituted derivatives. The electron distribution patterns in HOMO and LUMO states of **64** and **65** predicted that while the HOMO states of both the molecules are superimposable in the BODIPY core, the LUMO states indicate more delocalization towards 3,5-diformyl groups in **64** (Fig. 50), leading to electron deficient BODIPY core facilitating its reduction, thus pointing towards the important role of formyl groups in pH sensitivity of **64**.

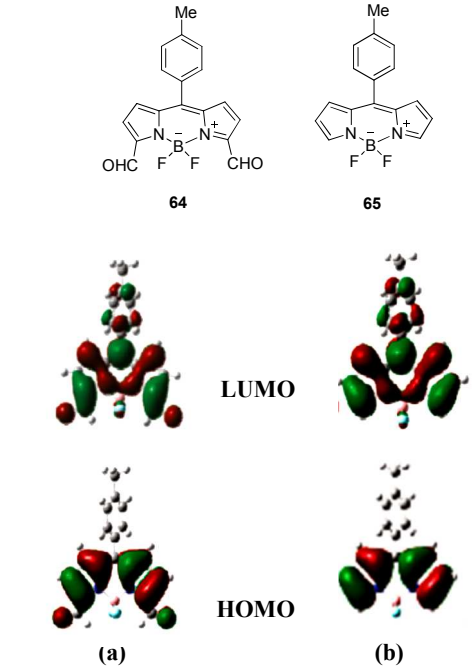

Fig. 50 Electron density distribution patterns in HOMO and LUMO states of (a) **64** and (b) **65** [Reprinted with permission from (ref. 40). Copyright (2011) American Chemical Society].

4.2 CT based system

The phosphorescent transition metal complexes, equipped with significant Stokes shifts, luminescence in the visible region and long lifetimes have attracted a great interest as the basic building blocks for the development of phosphorescence based chemosensors. In this context, the iridium(III) complexes have attained an important place in the family of phosphorescence dyes.[41] Working in this line, a cyclometallated iridium(III) complex **66** was employed for the detection of thiols.[42] The complex manifested its selectivity towards thiol in the form of hypsochromic shift in the low energy absorption band and

This journal is © The Royal Society of Chemistry [year]

RSC Advances Accepted Manuscript

enhanced emission. The DFT calculations have rendered the conversion of mainly intraligand (ILCT) transition in **66** to the MLCT/LLCT states in its adduct with cysteine, as a primary cause for the observed experimental changes.

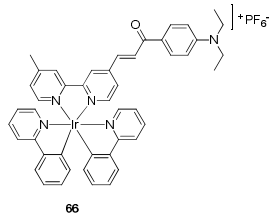

66

In addition to the above examples, we have recently reported[43,44] sensing properties of a quinolone based derivative **67**, which detected Hg^{2+}, Cu^{2+}, Fe^{3+}, as well as HSO_4^-. The unique feature was that it discriminated between cations and anions through binding at two different sites, thus constituting one of the rare examples of the receptors of this type. The proposed binding modes on the basis of various experimental studies have been well corroborated by DFT calculations. These calculations were suggestive of the involvement of the quinolone nitrogen in binding to the metal ions, and the response was observed at different energies, leading to the distinctive recognition, whereas trapping of HSO_4^- ion is accomplished through intermolecular hydrogen bonding interactions between the C-4 NH substituent [N-H--O (d_{H--O} = 2.21Å, angle NHO = 154.99º)] and C-5H [d_{O--H} = 2.77Å, angle CHO = 104.48º], of the quinolone moiety (Fig. 51).

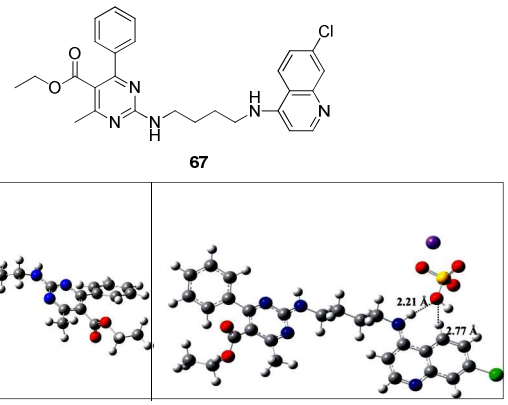

67

(a) **(b)**

Fig. 51 Energy minimised structures of (a) **67**:Cu^{2+} and (b) **67**:HSO_4^-. [Reproduced with permission from ref. 44. Copyright (2013) Royal Society of Chemistry].

5. Computational methods

The computational methods used in these investigations include: Hartree-Fock (HF)[27], Density Functional Theory (DFT)[27], DMol3[3] approach, atoms-in-molecules (AIM) calculations using the Gaussian 98/03/09 suite of programmes[2,23,27], MOPAC 2007 software[15], AIM2000 software[21], Materials Studio 4.2 or 4.4 package[3,4], Turbomole 5.9.0 programme package[14], Win MOPAC 3.0 [26], AMBER programme[22] etc. The various functionals used for the calculations include the Becke's three parameterised Lee-Yang-Par (B3LYP) exchange function[27], Becke-Perdew 86 (BP86) function[14], Perdew-Burke-Ernzerhof (PBE) function of generalised gradient approximation (GGA) level[3], meta-hybrid functional MO6-2X[34] and Truhlar's hybrid meta functional mPW1B95[20] For metals, such as Zn, Hg, Pb, Cu, Ag, Cs etc., LanL2DZ[21], Stuttgart-Dresden (SDD)[18], def2-SVP[14], Stuttgart relativistic small core (STRSC)[15] basis sets with effective core potential were employed, whereas for all other atoms, 3-21G[22], 6-31G[21], TZVP[31] basis sets were used with diffuse and polarization functions added in some cases. In case of donor atoms (N, O, F), basis set with added diffuse functions denoted as aug-cc-pVTZ[12] is used. The solvent effects were studied by using either the Cossi or Barone' CPCM (Conductor-like polarisable continuum model) modification of the Tomasi's PCM formalism[21] or the counterpoise approach or the COSMO method[15] by semiempirical level. Bond orders were characterised by the Wiberg bond index[15] (WBI) and calculated with the Natural Bond Orbital (NBO) population analysis[25], as the sum of squares of the off-diagonal density matrix elements between atoms. Atomic charge calculations were performed using Natural Population analysis (NPA)[22] and Natural Bond Orbital (NBO) population analysis[15]. The non-relativistic gauge-including atomic orbital (GIAO)[25] approach was employed to obtain the magnetic shielding tensor. The TD-DFT calculations were performed on the same method as used for the respective geometry optimisation. In order to search for significant bond critical points (BCPs) around the spatial region where weak host-guest interactions are taking place, Bader's AIM (atoms-in-molecules) methodology[15] was used.

6. Summary and perspective

This review presents a representative compilation of sensing events where the mechanism of the sensing event has been explained by a rational corroboration by the theoretical support. A comparable sketch of the sensing profiles of the chemosensing events discussed in the review is presented in Table 3. Theoretical calculations have become indispensable tools to corroborate the experimental data related to the electronic changes that accompany a sensing event for different analytes and explains the fundamental aspects concerning the modulation of different electronic states and energies, which in turn help in the search for more efficient sensors in terms of sensitivity, selectivity as well as improved detection limit, the important features for the success of the chemosensor action. Additionally these predictions can not only be helpful in reducing the amount of trials and errors in the development of efficient sensors, but can also lead to significant potential savings in time and resources to be consumed in synthesis of the sensors. This has well been demonstrated by L. Wang et.al[45] who have successfully employed this approach to develop fluorescent sensors for Zn^{2+}. Recently, R. Jin[46], in one of the interesting investigations has studied the interactions between diketopyrrole based derivatives and different halides using theoretical calculations and has established that the substituted derivatives can turn out to be efficient sensing materials.

Acknowledgements

The authors thank CSIR New Delhi for financial assistance (Projects: 01/2687/12-EMR-II) and UGC, New Delhi for the SAP project.

RSC Advances Accepted Manuscript

Notes and References

Department of Chemistry, Centre of Advance Study-1, Guru Nanak Dev University, Amritsar, India. Fax:91 1832258820; Tel:91 183 2258802-09 (Extn. 3508); E-mail: paramjit19in@yahoo.co.in and kamaljit19in@yahoo.co.in.

1 A. P. de Siva, H. Q. Nimal Gunaratne, T. Gunnlaugsson, A. J. M. Huxley, C. P. McCoy, J. T. Rademacher and T. E. Rice, *Chem. Rev.*, 1997, 97, 1515-1566.

2 H. S. Jung, P. S. Kwon, J. W. Lee, J. I. Kim, C. S. Hong, J. W. Kim, S. Yan, J. Y. lee, J. H. Lee, T. Joo and J. S. Kim, *J. Am. Chem. Soc.*, 2009,131, 2008-2012.

3 J. S. Bae, S-Y. Gwon, Y-A. Son and S-H. Kim, *Dyes and Pigments*, 2009, 83, 324-327.

4 Y.-A Son, S.-Y. Gwon and S.-H. Kim, *Mol. Cryst. Liq. Cryst.,* 2011, 538, 327-332.

5 T. Abalos, M. Moragues, S. Royo, D. Jimenez, R. Martinez-Manez, J. soto, F. Sancenon, S. Gil and J. Cano, *Eur. J. Inorg. Chem.* 2012, 76-84.

6 P. Kaur and D. Sareen, *Dyes Pigm.,* 2011, 88, 296.

7. P. Kaur, D. Sareen and K. Singh, *Talanta*, 2011, 83, 1695.

8 P. Kaur, D. Sareen and K. Singh, *Dalton Trans.,* 2012, 41 (29), 8767-8769.

9 P. Kaur, D. Sareen and K. Singh, *Anal. Chimica Acta,* 2013, 778, 79-86.

10 P. Kaur, S. Kaur, Y. Kasetti, P. V. Bharatam and K. Singh, *Talanta,* 2010, 83, 644-650.

11 J. Lim, T. A. Albright, B. R. Martin and O. S. Miljanic, *J. Org. Chem.* 2011, 76, 10207-10219.

12 Z. Yan, L. Hu, L. Nie and H. Lv, *Spectrochimica Acta part A,* 2011, 79, 661-665.

13 D. Ray, A. Nag, A. Jana, D. Goswami and P. K. Bharadwaj, *Inorg. Chim. Acta,* 2010, 363, 2824-2832.

14 S. Voutsadaki, G. K. Tsikalas, E. Klontzas, G. E. Froudakis and H. E. Katerinopoulos, *Chem. Commun.* 2010, 46, 3292-3294.

15 R. Martinez, A. Espinosa, A. Tarraga and P. Molina, *Tetrahedron,* 2010, 66, 3662-3667.

16 W.-C. Lin, C.-Y. Wu, Z.-H. Liu, C.-Y. Lin and Y.-P. Yen, *Talanta*, 2010, 81, 1209-1215.

17 Y.-C. Hsieh, J.-L. Chir, S.-T. Yang, S.-J. Chen, C.-H. Hu and A.-T. Wu, *Carbohydrate Res.,* 2011, 346, 978-981.

18 X. Wang, Z. Liu, F. Qian and W. He, *Inorg. Chem. Comm.,* 2012, 15, 176-179.

19 M. Hu, J. Fan, J. Cao, K. Song, H. Zhang, S. Sun and X. Peng, *Analyst,* 2012, 137, 2107-2111.

20 (a) F. Zapata, A. Caballero, A. Espinosa, A. Tarraga and P. Molina, *J. Org. Chem.*, 2009, 74, 4787-4796, (b) Y. Zhao and D. G. Truhlar, *J. Phys. Chem. A*, 2004, 108, 6908-6918, (c) Y. Zhao and D. G. Truhlar, *J. Phys. Chem. A*, 2005, 109, 5656-5667, (d) J. Muniz, L. E. Sansores, A. Martinez and R. Salcedo, *J. Mol. Struct.*, 2007, 820, 141-147.

21 F. Zapata, a. Caballero, A. Espinosa, a. Tarraga and P. Molina, *Inorg. Chem.*, 2009, 48, 11566-11576.

22 H. S. Jung, M. Park, D. Y. Han, E. Kim, C. Lee S. Ham and J. S. Kim, *Org. Lett.*, 2009, 11, 3378-3381.

23 L. Huang, J. Cheng, K. Xie, P. Xi, F. Hou, Z. Li, G. Xie, Y. Shi, H. Liu, D. Bai and Z. Zeng, *Dalton Trans,* 2011, 40, 10815-10817.

24 Y. Ding, X. Li, T. Li, W. Zhu and Y. Xie, *J. Org. Chem.*, 2013, 78, 5328-5338.

25 T. Romero, A. Caballero, A. Espinosa, A. Tarraga and P. Molina, *Dalton Trans,* 2009, 2121-2129.

26 Y. Shiraishi, K. Adachi, M. Itoh and T. Hirai, *Org. Lett.*, 2009, 11, 3482-3485.

27 Y. Sun, Y. Liu and W. Guo, *Sensors and Actuators B: Chemical,* 2009, 143, 171-176.

28 C. R. Wade and F. P. Gabbai, *Dalton Trans.,* 2009, 9169-9175.

29 R. Koteeswari, P. AshokKumar, V. T. Ramakrishnan, E. J. PadmaMalar and P. Ramamurthy, *Chem. Commun.,* 2010, 46, 3268-3270.

30 Z. Liu, X. Wang, Z. Yang and W. He, *J. Org. Chem.,* 2011, 76, 10286-10290.

31 G.-Y. Li, G.-J. Zhao, K.-L. Han and G.-Z. He, *J. Comput. Chem.,* 2011, 32, 668-674.

32 G.-Y. Li, G.-J. Zhao, Y.-H. Liu, K.-L. Han and G.-Z. He, *J. Comput. Chem.,* 2010, 31, 1759-1765.

33 Y. Peng, Y.-M. Dong, M. Dong and Y.-W. Wang, *J. Org. Chem.*, 2011, 77, 9072-9080.

34 P. Sokkalingam, D. S. Kim, H. Hwang, J. L. Sessler and C.-H. Lee, *Chemical Sci.,* 2012, 3, 1819-1824.

35 H. Lu, Q. Wang, Z. Li, G. Lai, J. Jiang and Z. Shen, *Org. Biomol. Chem.* 2011, 9, 4558-4562.

36 L. Deng, W. Wu, H. Guo, J. Zhao, S. Ji, X. Zhang, X. Yuan and C. Zhang, *J. Org. Chem.,* 2011, 76, 9294-9304.

37 Y. Zhou, J. Won, J. Y. Lee and J. Yoon, *Chem. Commun*., 2011, 47, 1997-1999.

38 J. V. Ros-Lis, R. Martinez-Manez, J. Soto, L. A. Villaescusa and K. Rurack, *J. Mater. Chem.,* 2011, 21, 5004-5010.

39 M. Hu, J. Fan, H. Li, K. Song, S. Wang, G. Cheng and X. Peng, *Org. Biomol. Chem.,* 2011, 9, 980-983.

40 S. Madhu, M. R. Rao, M. S. Shaikh and M. Ravikanth, *Inorg. Chem.,* 2011, 50, 4392-4400.

41 (a) K. M. C. Wong and V. W. W. Yam, *Coord. Chem. Rev.,* 2007, 251, 2477, (b) D. L. Ma, W. L. Wong, W. H. Chung, F. Y. Chan, P. K. So, T. S. Lai, Z. Y. Zhou, Y. C. Leung and K. Y. Wong, *Angew. Chem. Int. Ed.,* 2008, 47, 3735, (c) K. Huang, H. Yang, Z. Zhou, H. Chen, F. Li, T. Yi and C. Huang, *Inorg. Chim. Acta*, 2009, 362, 2577.

42 N. Zhao, Y.-H. Wu, L.-X. Shi, Q.-P. Lin and Z.-N. Chen, *Dalton Trans,* 2010, 39, 8288-8295.

43 P. Kaur, H. Kaur and K. Singh, *RSC Advances,* 2013, 3, 64-67.

44 P. Kaur, H. Kaur and K. Singh, *Analyst,* 2013, 138, 425-428.

45 (a) G. A. Hudson, L. Chang, J. Yu, Y. Yan, D. J. Dyer, M. E. McCarroll and L. Wang, *J. Phys. Chem. B*, 2010, 114, 870-876, (b) M. E. McCarroll, Y. Shi, S. Harris, S. Puli, I. Kimaru, R. Xu, L. Wang and D. Dyer, *J. Phys. Chem. B*, 2006, 110, 22991-22994.

46 R. Jin, *Theor. Chem. Acc.*, 2012, 131:1260.

RSC Advances Accepted Manuscript

This journal is © The Royal Society of Chemistry [year]

Table 3 Absorption, emission and/or redox changes and limit of detection upon recognition of analyte by the chemosensors reported in this review.

Compound	Analyte (medium, pH)	Absorption[a] $\Delta\lambda_{max}$ (nm)	Color change	Emission Change[b]	Redox change $\Delta E_{1/2}$ (mV)[c]	LOD[d]	Ref
1	Cu^{2+} (H_2O, 4-10)	15 R	Yellow to dark yellow	Quenched	-	0.5μM	2
2	Hg^{2+} (DMSO:H_2O, 9:1 v/v)	Intensity decreases	Yellow to colorless	Quenched	-	-	3
3	Ni^{2+} (CH_3CN)	83 B	-	Quenched (inhibited ICT)	-	-	4
4	Hg^{2+} (CH_3CN)	52 R	violet to blue	-	-	-	5
	Fe^{3+}(CH_3CN)	12B	Violet to red magenta	-	-	-	
10	Hg^{2+} (CH_3CN:H_2O, 9:1, v/v)	51-84 R	Yellow to purple	-	-	-	6
	Fe^{3+} (CH_3CN:H_2O, 9:1, v/v)	51-84 R	Yellow to red	-	-	-	
11	Cu^{2+} (CH_3CN:H_2O, 9:1, v/v)	119 R	Yellow to purple	-	-	1.36 x 10^{-5} M	7
12	Hg^{2+} (CH_3CN:H_2O, 9:1, v/v)	45-83 R	Orange to purple	-	0.08 AS	5.0 x 10^{-6} M	8
	Pb^{2+} (CH_3CN:H_2O, 9:1, v/v)	113 B	Orange to light yellow	-	0.05 AS		
13	Cu^{2+} (CH_3CN:H_2O, 9:1, v/v)	125 B	Orange to light yellow	-	-	9.0 x 10^{-6} M	9
	Co^{2+} (CH_3CN:H_2O, 9:1, v/v)	107 B	Orange to light green	--	-	10^{-5} M	
	Hg^{2+} (CH_3CN:H_2O, 9:1, v/v)	77 B	Orange to light green	-	-	10^{-5} M	
14	Hg^{2+} (CH_3CN:H_2O, 1:1, v/v, 7.0)	LEB vanishes HEB 34 R	Blue to colorless	-	-	-	10
16	Hg^{2+} (H_2O, 4.0-9.0)	LEB 54 R	-	-		2.9 x 10^{-8} M	12
17	Mg^{2+} [C_2H_5OH (abs.), CH_3CN (em.)]	107 R	-	Enhanced	-	-	13
18	Zn^{2+} [(C_2H_5OH (abs.), CH_3CN (em.)]	60 R	-	$\Delta\lambda_{em.}$=15 nm, R, enhanced	-	-	13
19	Hg^{2+} (H_2O, 7.0)	-	-	Enhanced, due to PET	-	-	14
21	Hg^{2+} (CH_3CN)	LEB at 528 nm and disappearance of HEB at 233-393	Yellowish to deep pink	CHEF = 12	-	2.5 x 10^{-6} M	15
	Cu^{2+} (CH_3CN)			CHEF = 27	-	4.5 x 10^{-6} M	
22	Hg^{2+} (DMSO:H_2O, 4:1, v/v, 7.8)	LEB 25 R HEB 3 B	Pale yellow to brown	enhanced	-	10^{-4} M (0.09 ppm)[e]	16
	Cu^{2+} (DMSO:H_2O, 4:1, v/v, 7.8)	Intensity of absorption peaks enhanced	Pale yellow to green yellow	enhanced	-	10^{-4} (0.10 ppm)[e]	
23	Cu^{2+} (CH_3OH)	-	-	Enhanced	-	1.3 x 10^{-4} M	17
	Hg^{2+} (CH_3OH)	-	-	Enhanced	-	1.26 x 10^{-5} M	
24	Zn^{2+} (CH_3CN)	36 R	-	$\Delta\lambda_{em.}$=51 nm, R, enhanced	-	-	18
25	Ag^{+} (H_2O, 7.4)	-	-	Enhanced	-	-	19
	Hg^{2+} (H_2O, 7.4)	-	-				
26	Pb^{2+} (CH_3CN:H_2O)	LEB 44 R HEB 11 R	Colorless to orange	CHEF	150 AS	1.32 x 10^{-8} M	20a
27	Pb^{2+} (CH_3CN:H_2O)	LEB 23 R	Pale orange to red	CHEF	120 AS	2.5 x 10^{-6} M	20a
28	Pb^{2+} (CH_3CN:H_2O)	LEB 23 R	Colorless to yellow	$\Delta\lambda_{em.}$=39 nm, R, CHEF	180 AS	1.32 x 10^{-8} M	20a
29	Pb^{2+} (CH_3CN:H_2O)	LEB 7 B HEB 160 B	-	$\Delta\lambda_{em.}$=10 nm, R, CHEF	110 AS	4.5 x 10^{-6} M	20a
30	Zn^{2+} (CH_3CN)	LEB 42 R	Orange to purple	CHEF = 184	10 AS	10^{-6} M	21
	Hg^{2+} (H_2O)	LEB 112 R	Orange to deep green	CHEF = 204	90 AS	10^{-6} M	
	Pb^{2+} (CH_3CN)	LEB 40 R	Orange to purple	CHEF = 90	10 AS	10^{-6} M	
31	Cu^{2+} (CH_3CN)	-	Colorless to orange	Formation of a new *excimer* band	-	10^{-6} M	22
34	Cu^{2+} (H_2O:DMSO, 9:1, v/v, 5.0-8.0)	39 R	--	quenched	-	0.1μM	23
38	Hg^{2+} (CH_3CN)	LEB 120 R HEB 70 R	Orange to deep red	-	210 mV AS	-	25
39	CN^{-} (H_2O:CH_3CN,	98 B	Pink to yellow	-	-	1.7 μM	26

RSC Advances Accepted Manuscript

	1:1, 9.3)						
40	CN^- (DMSO:H_2O, 1:1, v/v)	40 R	No change	$\Delta\lambda_{em.}$=14 nm, B, enhanced	-	5.6 x 10^{-8}M	27
41	CN^- (DMSO:H_2O, 1:1, v/v)	New band at 525 nm	Pale yellow to dark red	-	-	1.5 x 10^{-6} M	27
42	F^- (H_2O:$CHCl_3$)	LEB 49 R	Colorless to yellow	-	-	-	28
43	F^- (H_2O:$CHCl_3$)	LEB 75 R	Colorless to yellow	-	-	-	28
44	F^- (CH_3CN)	8 B followed by 17 R	-	$\Delta\lambda_{em.}$=120 nm, R, enhanced	-	-	29
45	CN^- (CH_3CN:H_2O, 95:5, v/v)	LEB 72 B	-	$\Delta\lambda_{em.}$=55 nm, B, enhanced	-	1.47 x 10^{-6} M	30
51	$HP_2O_7^{3-}$ (CH_3CN)	-	-	Enhanced	-	2 ppb	34
52	F^- (THF)	LEB 19 B HEB 18 B	Light green to colorless	$\lambda_{em.}$ B	-	10^{-6}	35
54	Cysteine (CH_3CN:H_2O, 4:1, v/v)	44 B	Purple to yellow	$\Delta\lambda_{em.}$=126 nm, B	-	-	36
56	Lysine [CH_3CN:HEPES buffer (pH 7.4, 0.01 M), 1:9, v/v)]	Enhanced broad band at 500 nm	Light yellow to pink	Enhanced	-	-	37
58	Propylamine and propylthio	Vanishes	Bleaching	-	-	-	38
62	Cys./HCys. (CH_3CN:HEPES 3:7,v/v, 7.4)	70 B	Orange to yellow	Enhanced	-	6.8 x 10^{-7} M	39
64	pH (acetate buffer soln., over a pH range of 4-9)	0, intensity increases with increasing H^+ ion concentration	--	*"on/off"*	-	-	40
66	Thiol (cysteine) [DMF:HEPES buffer (pH 7.2), 4:1, v/v)]	100 B	Yellow to colorless	Enhanced	-	-	42
67	Fe^{3+} (CH_3OH:H_2O, 9:1, 7.4)	LEB 0-13 R	-	94% quenched	-	9.24 x 10^{-5} M	43
	Cu^{2+} (CH_3OH:H_2O, 9:1, 7.4)	LEB 0-13 R	-	69% quenched	-	4.17 x 10^{-4} M	
	Hg^{2+} (CH_3OH:H_2O, 9:1, 7.4)		-	87% quenched	-	2.94 x 10^{-4} M	
	HSO_4^- (CH_3OH:H_2O, 9:1)	LEB 12 R	-	Quenched	-	-	44

[a]R=Red shift, B= Blue shift, LEB=Low energy band, HEB=High energy band; [b]CHEF-chelation enhanced fluorescence, PET- Photoinduced electron transfer; [c]AS = anodic shift; [d]LOD = Limit of detection, [e]LOD based on emission studies.

RSC Advances Accepted Manuscript

This journal is © The Royal Society of Chemistry [year]

Table of Content

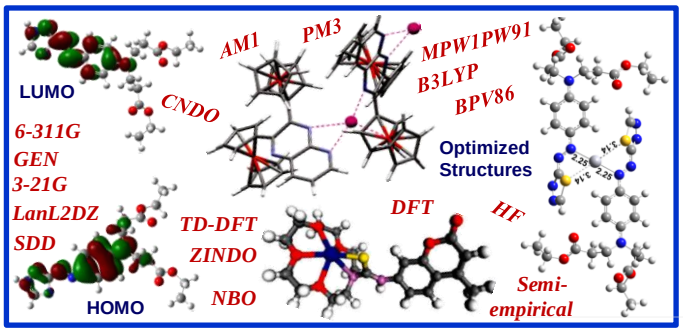

RSC Advances Accepted Manuscript